

- Kogler H, Hartmann O, Leineweber K, Nguyen P, Schott P, Brodde OE, Hasenfuss G. 2003. Mechanical load-dependent regulation of gene expression in monocrotaline-induced right ventricular hypertrophy in the rat. *Circ Res* 93:230–237.
- Levy D, Garrison RJ, Savage DD, Kannel WB, Castell WP. 1990. Prognostic implications of echocardiographically determined left ventricular mass in the Framingham Heart Study. *N Engl J Med* 322:1561–1566.
- Luo W, Wolska BM, Grupp IL, Harrer J, Ponniah S, Grupp G, Duffy JJ, Doetschman T, Kranias EG. 1994. Targeted ablation of the phospholamban gene is associated with markedly enhanced myocardial contractility and loss of beta-agonist stimulation. *Circ Res* 75:401–409.
- Luo W, Wolska BM, Grupp IL, Harrer JM, Haghghi K, Ferguson DG, Slack JP, Grupp G, Doetschman T, Solaro RJ, Kranias EG. 1996. Phospholamban gene dosage effects in the mammalian heart. *Circ Res* 78:839–847.
- MacLennan DH, Kranias EG. 2003. Phospholamban: a crucial regulator of cardiac contractility. *Nat Rev Mol Cell Biol* 4:566–577.
- McTiernan CF, Bonnie H Lemster, Frye C, Brooks S, Combes A, Feldman AM. 1997. Interleukin-1 $\beta$  inhibits phospholamban gene expression in cultured cardiomyocytes. *Circ Res* 81:493–503.
- McTiernan CF, Frye CS, Lemster BH, Kinder EA, Ogletree-Hughes ML, Moravec CS, Feldman AM. 1999a. The human phospholamban gene: structure and expression. *Mol Cell Cardiol* 31:679–692.
- McTiernan CF, Lemster BH, Frye CS, Johns DC, Feldman AM. 1999b. Characterization of proximal transcription regulatory elements in the rat phospholamban promoter. *J Mol Cell Cardiol* 31:2137–2153.
- Meyer M, Schillinger W, Pieske B, Holubarsch C, Heilmann C, Posival H, Kuwajima G, Mikoshiba K, Just H, Hasenfuss G. 1995. Alterations of sarcoplasmic reticulum proteins in failing human dilated cardiomyopathy. *Circulation* 92:778–784.
- Mills GD, Kubo H, Harris DM, Berretta RM, Piacentino V III, Houser SR. 2006. Phosphorylation of phospholamban at threonine-17 reduces cardiac adrenergic contractile responsiveness in chronic pressure overload-induced hypertrophy. *Am J Physiol Heart Circ Physiol* 291: H61–H70.
- Minamisawa S, Sato Y, Tatsuguchi Y, Fujino T, Imamura S, Uetsuka Y, Nakazawa M, Matsuoka R. 2003. Mutation of the phospholamban promoter associated with hypertrophic cardiomyopathy. *Biochem Biophys Res Commun* 304:1–4.
- Muangmingsuk S, Ingram P, Gupta MP, Arcilla RA, Gupta M. 2000. Dexamethasone induced cardiac hypertrophy in newborn rats is accompanied by changes in myosin heavy chain phenotype and gene transcription. *Mol Cell Biochem* 209:165–173.
- Rao MK, Xu A, Narayanan N. 2001. Glucocorticoid modulation of protein phosphorylation and sarcoplasmic reticulum function in rat myocardium. *Am J Physiol Heart Circ Physiol* 281:H325–H333.
- Richardson P, McKenna W, Bristow M, Maisch B, Mautner B, O'Connell J, Olsen E, Thiene G, Goodwin J, Gyarsas I, Martin I, Nordet P. 1996. Report of the 1995 World Health Organization/International Society and Federation of Cardiology Task Force on the definition and classification of cardiomyopathies. *Circulation* 93:841–842.
- Schmitt JP, Kamisago M, Asahi M, Li GH, Ahmad F, Mende U, Kranias EG, MacLennan DH, Seidman JG, Seidman CE. 2003. Dilated cardiomyopathy and heart failure caused by a mutation in phospholamban. *Science* 299:1410–1413.
- Schoneveld OJ, Gaemers IC, Lamers WH. 2004. Mechanisms of glucocorticoid signalling. *Biochim Biophys Acta* 1680:114–128.
- Schulz V, Hendig D, Henjakovic M, Szliska C, Kleesiek K, Gotting C. 2006. Mutational analysis of the ABCC6 gene and the proximal ABCC6 gene promoter in German patients with pseudoxanthoma elasticum (PXE). *Hum Mutat* 27:831–844.
- Seidman JG, Seidman C. 2001. Genetic basis for cardiomyopathy from mutation identification to mechanistic paradigms. *Cell* 104:557–567.
- Simmerman HK, Jones LR. 1998. Phospholamban: protein structure, mechanism of action, and role in cardiac function. *Physiol Rev* 78: 921–947.
- Smith L, Smith JB. 1994. Regulation of sodium-calcium exchanger by glucocorticoid and growth factor in vascular smooth muscle. *J Biol Chem* 269:27527–27531.
- Zhao W, Uehara Y, Chu G, Song Q, Qian J, Young K, Kranias EG. 2004. Threonine-17 phosphorylation of phospholamban: a key determinant of frequency-dependent increase of cardiac contractility. *J Mol Cell Cardiol* 37:607–612.

## Alteration of *N*-glycosylation in the kidney in a mouse model of systemic lupus erythematosus: relative quantification of *N*-glycans using an isotope-tagging method

Noritaka Hashii,<sup>1,2</sup> Nana Kawasaki,<sup>1,2</sup> Satsuki Itoh,<sup>1</sup> Yukari Nakajima,<sup>1,2</sup> Toru Kawanishi<sup>1</sup> and Teruhide Yamaguchi<sup>1</sup>

<sup>1</sup>Division of Biological Chemistry and Biologicals, National Institute of Health Sciences, Setagaya-ku, Tokyo, Japan, and <sup>2</sup>Core Research for Evolutional Science and Technology (CREST), of the Japan Science and Technology Agency (JST), Kawaguchi City, Saitama, Japan

doi:10.1111/j.1365-2567.2008.02898.x

Received 19 March 2008; revised 28 May 2008; accepted 2 June 2008.

Correspondence: N. Kawasaki, Division of Biological Chemistry and Biologicals, National Institute of Health Sciences, 1-18-1 Kamiyoga, Setagaya-ku, Tokyo 158-8501, Japan. Email: nana@nih.go.jp  
Senior author: Teruhide Yamaguchi, email: yamaguch@nih.go.jp

### Introduction

Glycosylation is one of the most common post-translational modifications<sup>1,2</sup> and contributes to many biological processes, including protein folding, secretion, embryonic development and cell–cell interactions.<sup>3</sup> Alteration of glycosylation is associated with several diseases, including inflammatory responses and malignancies;<sup>4–6</sup> for instance, significant increases in fucosylation and branching are found in ovarian cancer and lung cancer.<sup>7</sup> Additionally, the carbohydrate structure changes from type I glycans (Galβ1-3GlaNAc) to type II glycans (Galβ1-4GalNAc) in

### Summary

Changes in the glycan structures of some glycoproteins have been observed in autoimmune diseases such as systemic lupus erythematosus (SLE) and rheumatoid arthritis. A deficiency of  $\alpha$ -mannosidase II, which is associated with branching in *N*-glycans, has been found to induce SLE-like glomerular nephritis in a mouse model. These findings suggest that the alteration of the glycosylation has some link with the development of SLE. An analysis of glycan alteration in the disordered tissues in SLE may lead to the development of improved diagnostic methods and may help to clarify the carbohydrate-related pathogenic mechanism of inflammation in SLE. In this study, a comprehensive and differential analysis of *N*-glycans in kidneys from SLE-model mice and control mice was performed by using the quantitative glycan profiling method that we have developed previously. In this method, a mixture of deuterium-labelled *N*-glycans from the kidneys of SLE-model mice and non-labelled *N*-glycans from kidneys of control mice was analysed by liquid chromatography/mass spectrometry. It was revealed that the low-molecular-mass glycans with simple structures, including agalactobiantennary and paucimannose-type oligosaccharides, markedly increased in the SLE-model mouse. On the other hand, fucosylated and galactosylated complex type glycans with high branching were decreased in the SLE-model mouse. These results suggest that the changes occurring in the *N*-glycan synthesis pathway may cause the aberrant glycosylations on not only specific glycoproteins but also on most of the glycoproteins in the SLE-model mouse. The changes in glycosylation might be involved in autoimmune pathogenesis in the model mouse kidney.

**Keywords:** isotope-tagging method; liquid chromatography/multiple-stage mass spectrometry; systemic lupus erythematosus

carcinoembryonic antigen in colon cancer.<sup>8</sup> Furthermore, an increase in biantennary oligosaccharides lacking galactose (Gal) was found on immunoglobulin G (IgG) in systemic lupus erythematosus (SLE) and rheumatoid arthritis,<sup>9–11</sup> and agalactoglycans are used for the early diagnosis of rheumatoid arthritis.<sup>12</sup>

Systemic lupus erythematosus is an autoimmune disease characterized as chronic and as a systemic disease, with symptoms such as kidney failure, arthritis and erythema. In addition to the known changes in glycosylation on IgG, there have been several reports on the association between glycosylation and inflammation in SLE and rheumatoid

arthritis.<sup>13–15</sup> A deficiency of  $\alpha$ -mannosidase II ( $\alpha$ M-II), which is associated with branching in *N*-glycans, has been found to induce human SLE-like glomerular nephritis in a mouse model.<sup>16</sup> Green *et al.* reported that branching structures of *N*-glycan in mammals are involved in protection against immune responses in autoimmune disease pathogenesis.<sup>17</sup> Although there is no direct evidence that alteration of glycosylation is the upstream event in the pathogenesis of SLE, these findings suggest that changes in the glycan structure may be involved in the inflammatory-related autoimmune disorder. Glycosylation analysis may lead to the development of improved diagnostic methods and may help to clarify the carbohydrate-related pathogenic mechanism of inflammation in SLE.

Mass spectrometry (MS) and liquid chromatography/mass spectrometry (LC/MS) are the most prevalent strategies for identifying disease-related glycans in glycomics.<sup>18–20</sup> Aberrant glycosylations in some disease samples have been found by comparing mass spectra or chromatograms between normal and disease samples; however, because of the tremendous heterogeneities of the sugar moiety in glycoprotein as well as the low reproducibility of LC/MS, accurate quantitative analysis is difficult using MS and LC/MS alone. To overcome these problems, we previously developed the stable isotope-tagging method for the quantitative profiling of glycans using 2-aminopyridine (AP).<sup>21</sup> After the glycans are released from sample and the reference glycoproteins are derivatized to pyridyl amino ( $d_0$ -PA) glycans and to tetra-deuterium-labelled pyridyl amino ( $d_4$ -PA) glycans, respectively, a mixture of both  $d_0$ -PA and  $d_4$ -PA glycans was subjected to LC/MS, and the levels of individual glycans were calculated from the intensity ratios of  $d_0$ -glycan and  $d_4$ -glycan molecular ions (Fig. 1a). Recently, alternative isotope-tagging methods using deuterium-labelled compounds, such as 2-aminobenzoic acid its derivatives, and permethylation, have been proposed by other groups.<sup>22–24</sup> All of these studies prove the utility of isotope-tagging methods for the quantitative analysis of glycosylation.

In the present study, we used the isotope-tagging method to analyse changes in *N*-glycosylation in the disordered kidney in an SLE mouse model. We used an MRL/MpJ-lpr/lpr (MRL-lpr) mouse which lacks the Fas antigen gene.<sup>25–27</sup> The MRL-lpr mouse is known to naturally develop SLE-like glomerular nephritis and is widely used in SLE studies. MRL/MpJ-+/+ (MRL+/+) mice were used as controls.

## Materials and methods

### Materials

The kidneys of the SLE-model mice (MRL-lpr) and control mice (MRL+/+) ( $n = 3$ ) were purchased from Japan SLC, Inc. (Hamamatsu, Japan). Thermolysin (EC 3.4.24.27), originating from *Bacillus thermoproteolyticus*

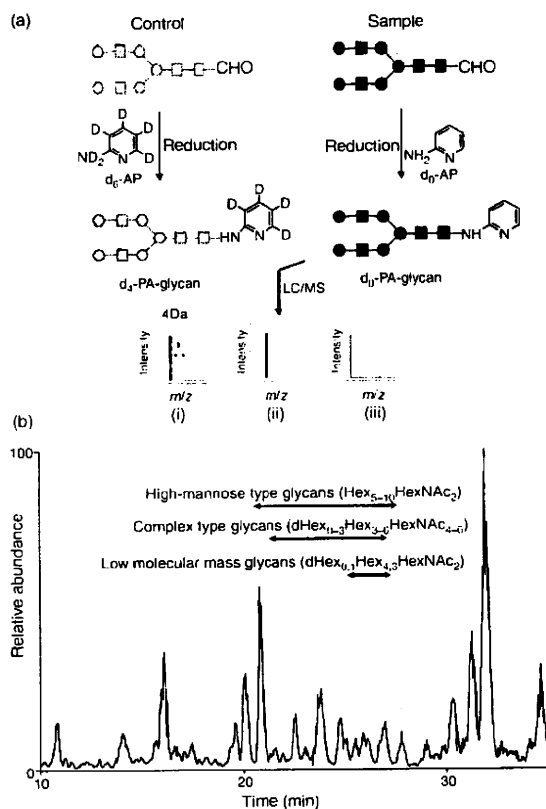


Figure 1. (a) Quantitative glycan profiling using the stable isotope-tagging method and liquid chromatography/mass spectrometry (LC/MS). (i) sample = control, (ii) sample > control, (iii) sample < control. (b) Total ion chromatogram obtained by a single scan ( $m/z$  700–2000) of the  $d_0$ -glycan and  $d_4$ -glycan mixture.

Rokko, was purchased from Daiwa Kasei (Shiga, Japan). Glycopeptidase A (PNGase A) was obtained from Seikagaku Kogyo Corporation (Tokyo, Japan). Non-deuterium-labelled 2-aminopyridine ( $d_0$ -AP) and deuterium-labelled 2-aminopyridine ( $d_6$ -AP) were purchased from Takara Bio (Otsu, Japan) and Cambridge Isotope Laboratories (Andover, MA), respectively.

### Sample preparation

Mouse kidneys were filtered using a cell strainer (70  $\mu$ m; BD Biosciences, San Jose, CA) and contaminating blood cells in the kidney cells were burst in 140 mM  $\text{NH}_4\text{Cl}$ -Tris buffer (pH 7.2). The surviving kidney cells were washed three times with phosphate-buffered saline containing a mixture of protease inhibitors (Wako, Tokyo, Japan) and dissolved in guanidine-HCl buffer (8 M guanidine-HCl, 0.5 M Tris-HCl, pH 8.6) containing a mixture of protease inhibitors by vortexing at 4°. The protein concentration was measured using a 2-D Quant Kit (GE Healthcare

Bio-Sciences, Uppsala, Sweden). The protein solution (200 µg proteins) was incubated with 40 mM dithiothreitol at 65° for 30 min. Freshly prepared sodium iodoacetate (final concentration, 96 mM) was added to the sample solution, and the mixture was incubated at room temperature for 40 min in the dark. The reaction was stopped by adding cystine (6 mg/ml in 2 M HCl) in an amount equal to the amount of dithiothreitol. The solution containing carboxymethylated proteins was diluted in four times its volume of H<sub>2</sub>O, and the mixture was incubated with 0.1 µg of thermolysin at 65° for 1 hr. After terminating the reaction by boiling, the reaction mixture was diluted in four times its volume of 0.2 M acetate buffer. The N-linked glycans were released by treatment with PNGase A (1 mU) at 37° for 16 hr and were desalted using an EnviCarb C cartridge (Supelco, Bellefonte, PA).

#### Labelling of N-glycans with d<sub>0</sub>-AP and d<sub>6</sub>-AP

Glycans released from the SLE-model mouse cells were incubated in acetic acid (20 µl) with 12.5 M d<sub>0</sub>-AP at 90° for 1 hr. Next, 3.3 M borane-dimethylamine complex reducing reagent in acetic acid (20 µl) was added to the solution and the mixture was incubated at 80° for 1 hr. Excess reagent was removed by evaporation, and d<sub>0</sub>-PA glycans were desalted using an EnviCarb C cartridge, concentrated in a SpeedVac and reconstituted in 20 µl of 5 mM ammonium acetate (pH 9.6). Glycans released from the control mouse were labelled with d<sub>6</sub>-AP in a similar manner. The resulting d<sub>4</sub>-PA glycans were combined with d<sub>0</sub>-PA glycans, which were prepared from an equal amount of proteins.

#### On-line liquid chromatography/mass spectrometry

The sample solution (4 µl) was injected into the LC/MS system through a 5-µl capillary loop. The d<sub>0</sub>-PA and d<sub>4</sub>-PA glycans were separated in a graphitized carbon column (Hypercarb, 150 × 0.2 mm, 5 µm; Thermo Fisher Scientific, Waltham, MA) at a flow rate of 2 µl/min in a Magic 2002 LC system (Michrom Bioresources, Auburn, CA). The mobile phases were 5 mM ammonium acetate containing 2% acetonitrile (pH 9.6, A buffer) and 5 mM ammonium acetate containing 90% acetonitrile (pH 9.6, B buffer). The PA-glycans were eluted with a linear gradient of 5–45% of B buffer for 90 min.

Mass spectrometric analysis of PA glycans was performed using a Fourier transform ion cyclotron resonance/ion trap mass spectrometer (FT-ICR-MS, LTQ-FT; Thermo Fisher Scientific) equipped with a nanoelectrospray ion source (AMR, Tokyo, Japan). For MS, the electrospray voltage was 2.0 kV in the positive ion mode, the capillary temperature was 200°, the collision energy was 25% for MS<sup>n</sup> experiment, and the maximum injection

times for FT-ICR-MS and MS<sup>n</sup> were 1250 and 50 milliseconds, respectively. The resolution of FT-ICR-MS was 50 000, the scan time (*m/z* 700–2000) was approximately 0.2 seconds, dynamic exclusion was 18 seconds, and the isolation width was 3.0 U (range of precursor ions ± 1.5).

## Results

### Quantitative profiling of kidney oligosaccharides in the SLE-model mouse

The recovery of oligosaccharides from whole tissues and cells is generally low because of the insolubility of the membrane fraction and possible degradation of the glycans. To improve the recovery of N-glycans from kidney cells, whole cells were dissolved in guanidine hydrochloride solution, and all proteins, including membrane proteins, were digested into peptides and glycopeptides with thermolysin. The N-glycans were then released from the glycopeptides with PNGase A, which is capable of liberating N-linked oligosaccharides even at the N- and/or C-terminals of peptides. The N-linked oligosaccharides from the SLE-model mice and control mice were labelled with d<sub>0</sub>-AP and d<sub>6</sub>-AP, respectively. The mixture of labelled glycans derived from an equal amount of proteins was subjected to quantitative glycan profiling using LC/MS<sup>n</sup>.

Figure 1(b) shows the total ion chromatogram obtained by a single mass scan (*m/z* 700–2000) of the glycan mixture in the positive ion mode. Although the MS data contain many MS spectra derived from contaminating low-molecular-weight peptides, the MS/MS spectra of oligosaccharides could be sorted based on the existence of carbohydrate-distinctive ions, such as HexHexNAc<sup>+</sup> (*m/z* 366) and Hex(dHex)HexNAc<sup>+</sup> (*m/z* 512). The mono-saccharide compositions of the precursor ions were calculated from accurate *m/z* values acquired by FT-ICR-MS. Oligosaccharides found at 25–27 min were assigned to low-molecular-mass glycans consisting of dHex<sub>0,1</sub>Hex<sub>4,5</sub>HexNAc<sub>2</sub> (dHex, deoxyhexose; Hex, hexose; HexNAc, N-acetylhexosamine). High-mannose-type glycans, which consist of Hex<sub>5–10</sub>HexNAc<sub>2</sub>, were located at 20–28 min; complex-type glycans (dHex<sub>0–3</sub>Hex<sub>3–6</sub>HexNAc<sub>4–6</sub>) were found at 21–27 min. Figure 2(a) shows the relative intensities of the molecular ions of N-glycans in the SLE-model mouse, which may correspond roughly to the levels of individual N-glycans. More than half of all glycans were complex-type oligosaccharides, and the most prominent glycan was dHex<sub>3</sub>Hex<sub>5</sub>HexNAc<sub>5</sub>. Man-9 (Hex<sub>9</sub>HexNAc<sub>2</sub>) was the second most common oligosaccharide. Nearly one-quarter of the glycans were low-molecular-mass glycans, and dHex<sub>1</sub>Hex<sub>3</sub>HexNAc<sub>2</sub> was the third most abundant glycan in the SLE-model mouse. The rate of percentage change in individual glycans between the SLE-model mice and control mice was calculated from the intensity ratio of d<sub>0</sub>-glycan and d<sub>4</sub>-glycan

Differential analysis of N-glycan in the kidney in a SLE mouse model

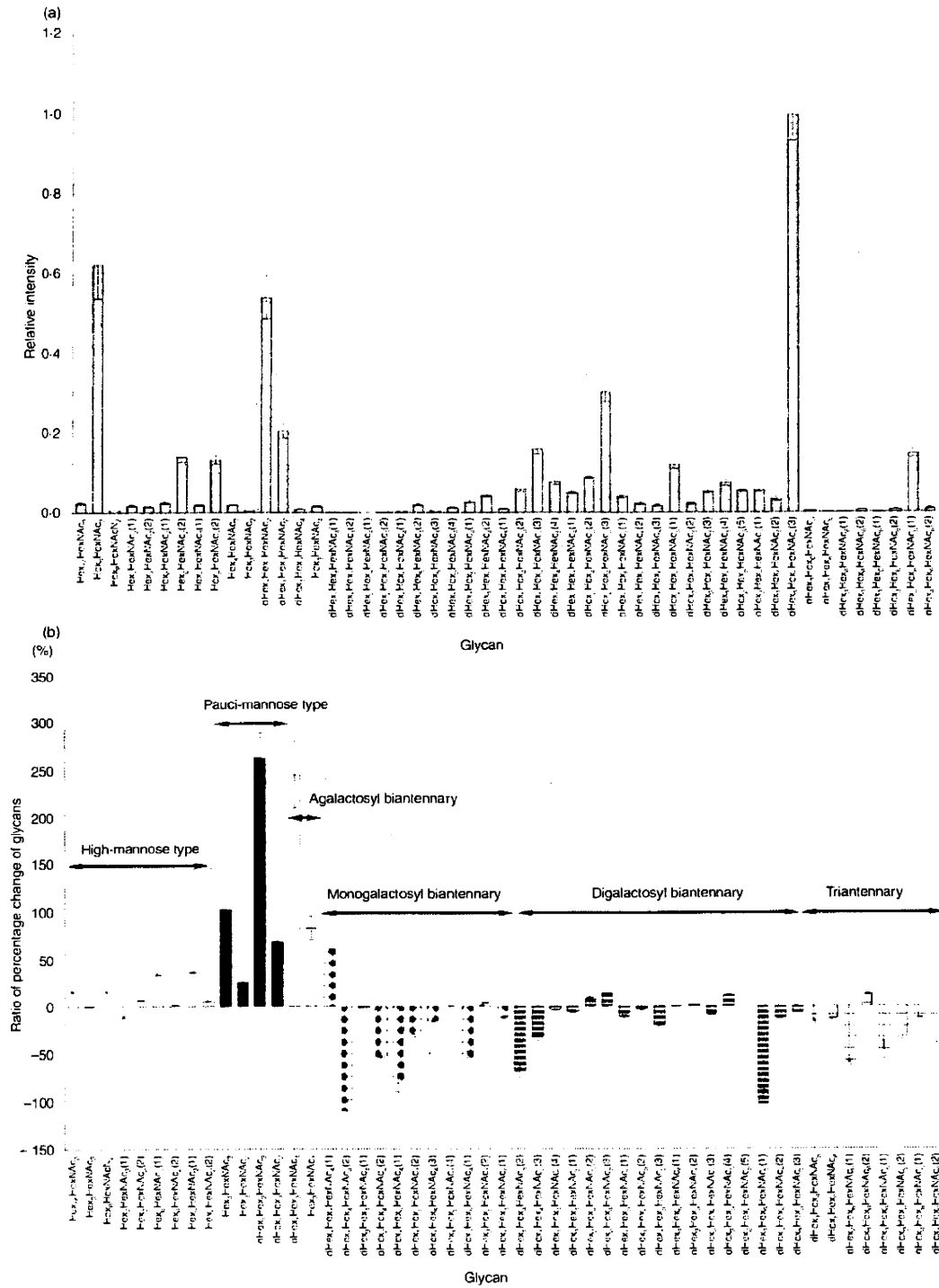


Figure 2. (a) Relative intensities of the molecular ions of  $d_0$ -pyridyl amino (PA) glycans from the systemic lupus erythematosus (SLE) model mouse. The intensity of the most intense ion ( $M + 2H_2^{2+}$  of  $d_4$ -PA  $dHex_3Hex_5HexNAc_3(3)$ ,  $m/z$  1180.97) was taken as 1.0. (b) Rate of percentage change of  $d_0/d_4$ -glycans. Each value is the average of three biological repeats. Error bars correspond to the standard deviation. The numbers in parentheses show the isomers.

molecular ions (Fig. 2b). The significant changes found in many glycans are described below.

**Increased oligosaccharides in the SLE-model mouse**

Figure 3(a,b) show the mass and MS/MS spectra of the most increased glycan, which showed a notable increase in the SLE-model mouse. Based on *m/z* values of molecular ions and differences of 1.00 U in *m/z* values among monoisotopic ions, the intense ion (*m/z* 973.40) and its neighbour ion (*m/z* 977.43) were assigned to [M+H]<sup>+</sup> of d<sub>0</sub>-PA dHex<sub>1</sub>Hex<sub>2</sub>HexNAC<sub>2</sub>, and d<sub>4</sub>-PA dHex<sub>1</sub>Hex<sub>2</sub>HexNAC<sub>2</sub>, respectively (Fig. 3a). The intensity ratio of these ions suggested that the level of dHex<sub>1</sub>Hex<sub>2</sub>HexNAC<sub>2</sub> increased 3.6-fold in the SLE-model mouse. The structure of this oligosaccharide was estimated to be a core-fucosylated trimannosyl core lacking a Man residue from the successive cleavages of Man (Y<sub>3</sub>: *m/z* 815), Man (Y<sub>2</sub>: *m/z* 653), GlcNAc (Y<sub>1</sub>: *m/z* 450) and Fuc (Y<sub>111</sub>: *m/z* 304) (inset in Fig. 3b). Such a defective N-glycan is known as a paucimannose-type glycan, and is rarely found in vertebrates. All paucimannose-type glycans, such as dHex<sub>1</sub>Hex<sub>3</sub>HexNAC<sub>2</sub> (a core-fucosylated trimannosyl core) and Hex<sub>3</sub>HexNAC<sub>2</sub> (a non-fucosylated trimannosyl core) were increased in the SLE-model mouse. Furthermore, a two-fold increase was found in Hex<sub>4</sub>HexNAC<sub>2</sub> (Man-4).

Figure 4 shows the molecular ratios of individual N-glycans between the SLE-model mice and control mice. A remarkable increase (3.5-fold) was also found in

dHex<sub>1</sub>Hex<sub>3</sub>HexNAC<sub>4</sub>, which is assigned to a core-fucosylated biantennary oligosaccharide lacking two non-reducing terminal Gal residues; its non-fucosylated form (Hex<sub>3</sub>HexNAC<sub>4</sub>) was also increased 1.8-fold in the SLE-model mouse. In other complex-type glycans, dHex<sub>1</sub>Hex<sub>4</sub>HexNAC<sub>4</sub> (1), which is assigned to a biantennary oligosaccharide lacking one molecule of Gal, increased 1.6-fold. Interestingly, a significant decrease was found in dHex<sub>1</sub>Hex<sub>4</sub>HexNAC<sub>4</sub> (2), a positional isomer of dHex<sub>1</sub>Hex<sub>4</sub>HexNAC<sub>4</sub> (1); this might have been caused by galactosylation on either GlcNAc-Man $\alpha$ 1-3 or GlcNAc-Man $\alpha$ 1-6. In contrast, no change was found between fucosylated and non-fucosylated oligosaccharides, nor between bisected and non-bisected oligosaccharides.

A significant increase was found in some high-mannose-type oligosaccharides, such as Hex<sub>2</sub>HexNAC<sub>2</sub> (Man-5; +137%) and Hex<sub>6</sub>HexNAC<sub>2</sub> (1) (Man-6; +136%), while Hex<sub>7</sub>HexNAC<sub>2</sub> (1,2) (Man-7) and a positional isomer of Hex<sub>6</sub>HexNAC<sub>2</sub> (1) [Hex<sub>6</sub>HexNAC<sub>2</sub> (2)] remained unchanged in the SLE-model mouse. A slight increase was found in Hex<sub>8</sub>HexNAC<sub>2</sub> (Man-8; +116%) and Hex<sub>10</sub>HexNAC<sub>2</sub> (possibly assigned to Man-9 plus Glc; +116%).

**Decreased oligosaccharides in the SLE-model mouse**

The mass spectrum of the most decreased glycan is shown in Fig. 5(a). Based on differences of 0.5 U in *m/z* values among monoisotopic ions, molecular ions at *m/z* 1180.97

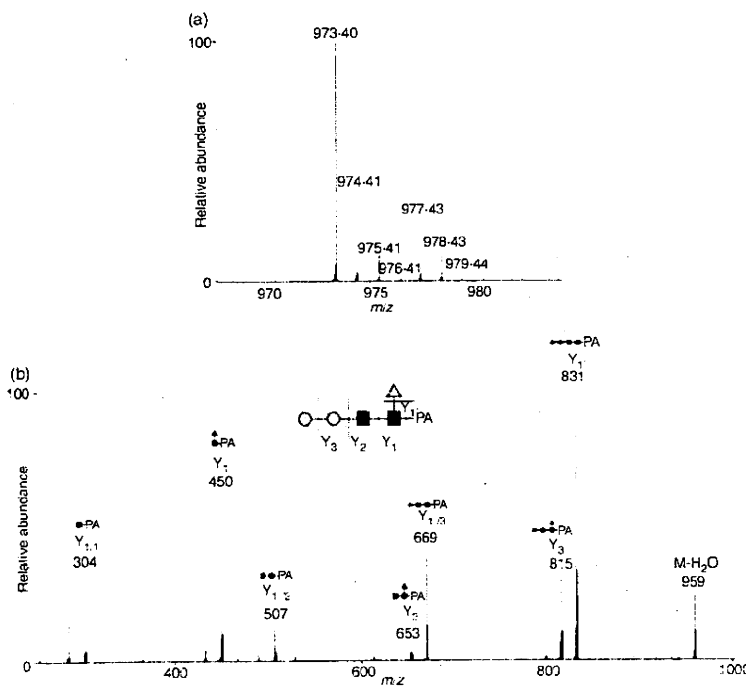


**Figure 3.** Mass (a) and mass spectrometry (MS)/MS (b) spectra of the most increased glycan (dHex<sub>1</sub>Hex<sub>2</sub>HexNAC<sub>2</sub>). Precursor ion, *m/z* 973.4; grey circle, mannose; grey triangle, fucose; black square, N-acetylglucosamine.

## Differential analysis of N-glycan in the kidney in a SLE mouse model

Increased glycan (>120%)	Deduced structure								
	Abbreviation	dHex1HexNAc1 (1)	dHex1Hex2HexNAc1 (1)	dHex1Hex3HexNAc1 (1)	dHex1Hex4HexNAc1 (1)	dHex1Hex2Hex3HexNAc1 (1)	dHex1Hex2Hex4HexNAc1 (1)	dHex1Hex3Hex4HexNAc1 (1)	dHex1Hex2Hex3Hex4HexNAc1 (1)
	Intensity ratio(%)	136	137	204	139	363	170	184	346
Decreased glycan (<-120%)	Deduced structure								
	Abbreviation	dHex1Hex2Hex3Hex4HexNAc1 (2)	dHex1Hex2Hex3Hex4Hex5HexNAc1 (1,2)	dHex1Hex2Hex3Hex4Hex5Hex6HexNAc1 (1,2)	dHex1Hex2Hex3Hex4Hex5Hex6Hex7HexNAc1 (2)	dHex1Hex2Hex3Hex4Hex5Hex6Hex7Hex8HexNAc1 (1,2)	dHex1Hex2Hex3Hex4Hex5Hex6Hex7Hex8Hex9HexNAc1 (1)	dHex1Hex2Hex3Hex4Hex5Hex6Hex7Hex8Hex9Hex10HexNAc1 (1,2)	dHex1Hex2Hex3Hex4Hex5Hex6Hex7Hex8Hex9Hex10Hex11HexNAc1 (2)
	Intensity ratio(%)	-208	-182, -133	-169, -133	-149	-154	-213	-159	-147, -132
Other glycan	Deduced structure								
	Abbreviation	dHex1Hex2Hex3Hex4Hex5Hex6Hex7Hex8Hex9Hex10Hex11Hex12HexNAc1 (2,3)	dHex1Hex2Hex3Hex4Hex5Hex6Hex7Hex8Hex9Hex10Hex11Hex12Hex13HexNAc1 (1)	dHex1Hex2Hex3Hex4Hex5Hex6Hex7Hex8Hex9Hex10Hex11Hex12Hex13Hex14HexNAc1 (1,2)	dHex1Hex2Hex3Hex4Hex5Hex6Hex7Hex8Hex9Hex10Hex11Hex12Hex13Hex14Hex15HexNAc1 (1,2)	dHex1Hex2Hex3Hex4Hex5Hex6Hex7Hex8Hex9Hex10Hex11Hex12Hex13Hex14Hex15Hex16HexNAc1 (2,3)	dHex1Hex2Hex3Hex4Hex5Hex6Hex7Hex8Hex9Hex10Hex11Hex12Hex13Hex14Hex15Hex16Hex17HexNAc1 (2)	dHex1Hex2Hex3Hex4Hex5Hex6Hex7Hex8Hex9Hex10Hex11Hex12Hex13Hex14Hex15Hex16Hex17Hex18HexNAc1 (1)	dHex1Hex2Hex3Hex4Hex5Hex6Hex7Hex8Hex9Hex10Hex11Hex12Hex13Hex14Hex15Hex16Hex17Hex18Hex19HexNAc1 (1)
	Intensity ratio (%)	116	101	116	-111, 107	102	106	-115, 101	-101
Other glycan	Deduced structure								
	Abbreviation	dHex1Hex2Hex3Hex4Hex5Hex6Hex7Hex8Hex9Hex10Hex11Hex12Hex13Hex14Hex15Hex16Hex17Hex18Hex19Hex20HexNAc1 (1,2)	dHex1Hex2Hex3Hex4Hex5Hex6Hex7Hex8Hex9Hex10Hex11Hex12Hex13Hex14Hex15Hex16Hex17Hex18Hex19Hex20Hex21HexNAc1 (1,2)	dHex1Hex2Hex3Hex4Hex5Hex6Hex7Hex8Hex9Hex10Hex11Hex12Hex13Hex14Hex15Hex16Hex17Hex18Hex19Hex20Hex21Hex22HexNAc1 (1,2)	dHex1Hex2Hex3Hex4Hex5Hex6Hex7Hex8Hex9Hex10Hex11Hex12Hex13Hex14Hex15Hex16Hex17Hex18Hex19Hex20Hex21Hex22Hex23HexNAc1 (1,2)	dHex1Hex2Hex3Hex4Hex5Hex6Hex7Hex8Hex9Hex10Hex11Hex12Hex13Hex14Hex15Hex16Hex17Hex18Hex19Hex20Hex21Hex22Hex23Hex24HexNAc1 (2,3)	dHex1Hex2Hex3Hex4Hex5Hex6Hex7Hex8Hex9Hex10Hex11Hex12Hex13Hex14Hex15Hex16Hex17Hex18Hex19Hex20Hex21Hex22Hex23Hex24Hex25HexNAc1 (1)	dHex1Hex2Hex3Hex4Hex5Hex6Hex7Hex8Hex9Hex10Hex11Hex12Hex13Hex14Hex15Hex16Hex17Hex18Hex19Hex20Hex21Hex22Hex23Hex24Hex25Hex26HexNAc1 (1)	dHex1Hex2Hex3Hex4Hex5Hex6Hex7Hex8Hex9Hex10Hex11Hex12Hex13Hex14Hex15Hex16Hex17Hex18Hex19Hex20Hex21Hex22Hex23Hex24Hex25Hex26Hex27HexNAc1 (1)
	Intensity ratio(%)	-104, -105	-111, -103, -119	-101, 102, -110, 113, 100	110, 115	-112	-106	-114	116

Figure 4. Summary of quantitative analysis of the systemic lupus erythematosus (SLE) model mouse against control mice. Values of relative ratios are the averages of three biological repeats. Grey circle, mannose; white circle, galactose; grey triangle, fucose; black square, N-acetylglucosamine.

and 1182.98 are estimated to be  $[M + 2H]^{2+}$  of  $d_0$ -PA and  $d_4$ -PA  $dHex_1Hex_5HexNAc_5$  (1), respectively. The intensity ratio of  $d_0 : d_4$  glycans suggests that this glycan in the SLE-model mouse was decreased to 47% of the amount found in the control mouse. Figure 5(b) shows the  $MS^{2-4}$  spectra of  $d_0$ -PA  $dHex_1Hex_5HexNAc_5$  (1) (precursor ion,  $m/z$  1180.97). The fragment ion at  $m/z$  512 in MS/MS (i) and MS/MS/MS (ii) spectra, which corresponds to  $dHex_1Hex_1HexNAc_1^+$ , suggests the attachment of two Lewis motifs on the side chains of the glycan. The presence of  $dHex_1HexNAc_1PA^+$  ( $m/z$  446) and  $dHex_1Hex_1HexNAc_3PA^+$  ( $m/z$  1015) reveals the linkages of a core fucose and a bisecting GlcNAc. Based on these fragments, this decreased glycan is estimated to be a Lewis-motif-modified, core-fucosylated and bisected biantennary oligosaccharide (inset in Fig. 5).

As shown in Figs 2(b) and 4, oligosaccharides lacking one molecule of Gal with and without bisecting GlcNAc [ $dHex_1Hex_4HexNAc_4$  (2) and  $dHex_1Hex_4HexNAc_3$  (1)] were decreased to 48% and 55%, respectively. A significant decrease was also found in other monogalacto-biantennary oligosaccharides, such as  $dHex_2Hex_4HexNAc_4$  (2) (a Lewis-motif-modified, core-fucosylated monogalacto-biantennary) and  $dHex_2Hex_4HexNAc_3$  (1) (a Lewis-motif-modified core-fucosylated and bisected monogalacto-biantennary).

The oligosaccharides, non-reducing ends of which are fully galactosylated, were decreased in the SLE-model mouse. For example, monofucosyl biantennary  $dHex_1Hex_3HexNAc_4$  (1) and (2) were decreased 59% and 75%, respectively. The di-, tri- and tetra-fucosylated oligosaccharides,  $dHex_2Hex_6HexNAc_6$  (1),  $dHex_3Hex_6HexNAc_6$  (1,2) and  $dHex_4Hex_6HexNAc_6$  (1,2), which were estimated to be tri- and tetraantennary forms, were also significantly decreased. These results show that oligosaccharides with a complicated structure, such as high branching oligosaccharides and di- and tri-fucosylated oligosaccharides, were decreased in the SLE-model mouse.

## Discussion

Using the isotope-tagging method, we demonstrated aberrant N-glycosylation on the kidney proteins of a SLE-model mouse. We found increases in low-molecular-mass glycans with simple structures, including paucimannose-type glycans, agalacto-biantennary oligosaccharides, Man-5 and Man-6, and decreases in glycans which have a complicated and diverse structure, such as digalacto-biantennary oligosaccharides and highly fucosylated glycans (Fig. 4). An increase in agalacto-biantennary oligosaccharides on IgG has been reported in the sera of patients with autoimmune diseases, including SLE, rheumatoid arthritis and IgA

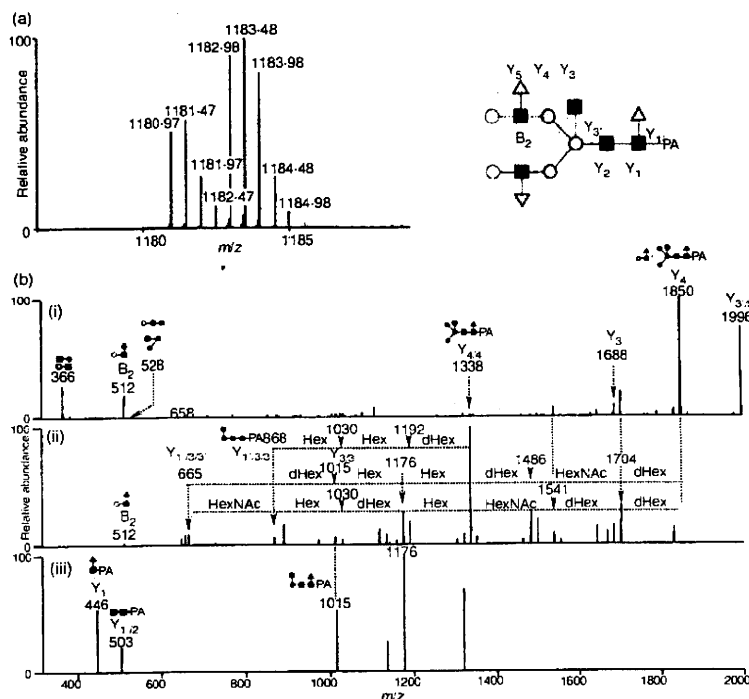


Figure 5. (a) Mass spectrum of the most decreased glycan [dHex<sub>4</sub>Hex<sub>3</sub>HexNAc<sub>3</sub> (1); (b-i) Mass spectrometry (MS)/MS spectrum of *m/z* 1181-0; (b-ii) MS/MS/MS spectrum of *m/z* 1849-7; (b-iii) MS/MS/MS/MS spectrum of *m/z* 1338-3. Grey circle, mannose; white circle, galactose; grey triangle, fucose; black square, N-acetylglucosamine; dHex, deoxyhexose (fucose); Hex, hexose (mannose and galactose); HN, N-acetylhexosamine (N-acetylglucosamine).

nephropathy.<sup>9,11,28</sup> The present findings show that abnormal glycosylation occurs not only in IgG in serum but also in several glycoproteins in the SLE-model mouse kidney.

Figure 6 shows the biosynthesis pathway of N-linked oligosaccharides in mammalian cells. Man-9, a product in the early stage of the pathway, is processed to Man-5 in the endoplasmic reticulum, and a GlcNAc and Fuc are added to Man-5 in the Golgi apparatus. After the removal of two Man residues by  $\alpha$ M-II, GlcNAc, Gal and Fuc are further added to oligosaccharides by several glycosyltransferases. There have been a few reports on paucimannose-type oligosaccharides in vertebrates;<sup>29</sup> however, these glycans are common oligosaccharides in other multicellular organisms such as insects and *Caenorhabditis*

*elegans*.<sup>30,31</sup> The membrane protease  $\beta$ -N-acetylglucosaminidase is thought to mediate the synthesis of paucimannose-type oligosaccharides.<sup>32</sup> Based on core fucosylation on some paucimannose-type oligosaccharides, it was deduced that  $\beta$ -N-acetylglucosaminidase might act on glycan synthesis after N-acetylglucosaminyltransferase I, core fucosyltransferase and  $\alpha$ M-II.<sup>32</sup> The synthesis of paucimannose-type oligosaccharides may be involved in the suppression of growing diversity and complexity of glycan structures.

We found a number of changes in the levels of monogalacto-biantennary oligosaccharides in the SLE mouse. Galactosylation to agalacto-biantennary oligosaccharides is mediated by  $\beta$ -1,4-galactosyltransferase

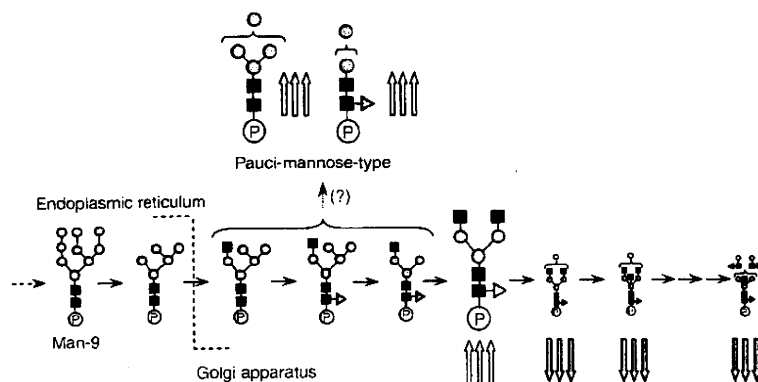


Figure 6. Biosynthesis pathway of N-linked oligosaccharides in mammalian cells. Triple up-arrow, increases of more than +2.0; triple down-arrow, decreases of not more than -2.0. Grey circle, mannose; white circle, galactose; grey triangle, fucose; black square, N-acetylglucosamine. 'P' is protein portion.



( $\beta$ -1,4-GalTase).<sup>33</sup> Previous studies suggested that transcriptional repression of  $\beta$ -1,4-GalTase in lymphocytes is associated with an increase in agalacto-oligosaccharides on IgG in the serum of the MRL-lpr mouse.<sup>34</sup> Although the activity of  $\beta$ -1,4-GalTase remains unknown in the SLE-model mouse, the increase in agalacto forms and the decrease in digalacto forms imply changes in  $\beta$ -1,4-GalTase activity. The present results suggest a decrease in diverse and complex glycans, which are synthesized at a late stage in the *N*-glycan synthesis pathway, and an increase in the simple glycans appearing at an early stage in the SLE-model mouse.

The activation of complements is involved in glomerular nephritis of SLE.<sup>35–37</sup> The complements are activated through three pathways: a classical pathway, an alternative pathway and a lectin pathway. In the classical pathway, a binding of C1q to an immune complex triggers the activation of C1r and C1s. Activated C1s cleaves C4 and C2, generating C3 convertase (C4b2a), which generates C3b. The complement component subsequently produces C5b-9 complex, which leads to an inflammatory response on host tissues.<sup>38–41</sup> The excess deposition of immune complexes followed by a sustained immune response triggers tissue disorders, including lupus nephritis.<sup>42–45</sup> In the lectin pathway, mannose-binding lectin (MBL) is associated with the activation of complements. Two forms of MBL (MBL-A and MBL-C) are present in complexes with MBL-associated serine proteases (MASPs) in mice. The MASPs are activated by binding MBL to Man or GlcNAc on the surface of the antigen in a calcium-dependent manner.<sup>46–49</sup> Like C1s in the classical pathway, activated MASPs cleave C4 and C2.<sup>50,51</sup> In lupus nephritis, MBL-A and MBL-C in the immune complex bind to GlcNAc residues at the reducing ends of agalacto-biantennary oligosaccharides in IgG,<sup>52</sup> and subsequently activate the complements.<sup>53,54</sup> In  $\alpha$ M-II-deficient mice, which suffer from SLE-like syndromes including kidney disorders, the majority of glycans are hybrid-type oligosaccharides because of the failure of Man trimming by the lack of  $\alpha$ M-II.<sup>16</sup> Green *et al.* concluded that MBL recognized Man $\alpha$ 1–3 and Man $\alpha$ 1–6 linkages in hybrid-type oligosaccharides,<sup>17</sup> and glycans lacking normal side chains, including agalacto-biantennary oligosaccharides, might be involved in the aberrant immune response in autoimmune diseases. Paucimannose glycans, which contain exposed Man $\alpha$ 1–3 or Man $\alpha$ 1–6 linkages, may be recognized as ligand carbohydrates by MBL. Our present finding, an increase in paucimannose oligosaccharides and agalacto forms, might result from an alteration of the biosynthesis pathway of *N*-glycans. The alterations may cause the aberrant glycosylations on most of the glycoproteins rather than some glycoproteins in the SLE-model mouse. The changes in glycosylation might be involved in an autoimmune pathogenesis in the SLE-model mouse kidney.

The continuous production of aberrant antibodies that react with components from self-tissue and accumulation in the immune complex are thought to promote tissue damage in autoimmune disease.<sup>55,56</sup> The mechanism of localized accumulation in the immune complex in some tissues remains unknown in SLE. We found an increase in glycans that may bind to MBL and subsequently promote complement activation via the lectin pathway in the mouse kidney. Our present results suggest that an aberrant *N*-glycan synthesis pathway as well as an abnormal immune system may be involved in the damage caused by glomerular nephritis in the SLE-model mouse.

### Acknowledgements

This study was supported in part by a Grant-in-Aid from the Ministry of Health, Labor, and Welfare, and Core Research for the Evolutional Science and Technology Program (CREST), Japan Science and Technology Corp (IST).

### References

- 1 Dwek RA. Glycobiology: toward understanding the function of sugars. *Chem Rev* 1996; **96**:683–720.
- 2 Helenius A, Aebi M. Intracellular functions of N-linked glycans. *Science* 2001; **291**:2364–9.
- 3 Zak I, Lewandowska E, Gnypl W. Selectin glycoprotein ligands. *Acta Biochim Pol* 2000; **47**:393–412.
- 4 Axford JS. Glycosylation and rheumatic disease. *Biochim Biophys Acta* 1999; **1455**:219–29.
- 5 Feizi T, Gooi HC, Childs RA, Picard JK, Uemura K, Loomes LM, Thorpe SJ, Hounsell EF. Tumour-associated and differentiation antigens on the carbohydrate moieties of mucin-type glycoproteins. *Biochem Soc Trans* 1984; **12**:591–6.
- 6 Kannagi R, Izawa M, Koike T, Miyazaki K, Kimura N. Carbohydrate-mediated cell adhesion in cancer metastasis and angiogenesis. *Cancer Sci* 2004; **95**:377–84.
- 7 Goodarzi MT, Turner GA. Decreased branching, increased fucosylation and changed sialylation of alpha-1-proteinase inhibitor in breast and ovarian cancer. *Clin Chim Acta* 1995; **236**:161–71.
- 8 Yamashita K, Fukushima K, Sakiyama T, Murata F, Kuroki M, Matsuoka Y. Expression of Sia alpha 2-6Gal beta 1-4GlcNAc residues on sugar chains of glycoproteins including carcinoembryonic antigens in human colon adenocarcinoma: applications of *Trichosanthes japonica* agglutinin I for early diagnosis. *Cancer Res* 1995; **55**:1675–9.
- 9 Tomana M, Schrohenloher RE, Reveille JD, Arnett FC, Koopman WI. Abnormal galactosylation of serum IgG in patients with systemic lupus erythematosus and members of families with high frequency of autoimmune diseases. *Rheumatol Int* 1992; **12**:191–4.
- 10 Mizuochi T, Hamako I, Nose M, Titani K. Structural changes in the oligosaccharide chains of IgG in autoimmune MRL/Mp-lpr/lpr mice. *J Immunol* 1990; **145**:1794–8.
- 11 Arnold IN, Wormald MR, Sim RB, Rudd PM, Dwek RA. The impact of glycosylation on the biological function and structure

- of human immunoglobulins. *Annu Rev Immunol* 2007; **25**:21–50.
- 12 Das H, Atsumi T, Fukushima Y *et al.* Diagnostic value of anti-galactosyl IgG antibodies in rheumatoid arthritis. *Clin Rheumatol* 2004; **23**:218–22.
  - 13 Raghav SK, Gupta B, Agrawal C, Saroha A, Das RH, Chaturvedi VP, Das HR. Altered expression and glycosylation of plasma proteins in rheumatoid arthritis. *Glycoconj J* 2006; **23**:167–73.
  - 14 Elliott MA, Elliott HG, Gallagher K, McGuire J, Field M, Smith KD. Investigation into the concanavalin A reactivity, fucosylation and oligosaccharide microheterogeneity of alpha 1-acid glycoprotein expressed in the sera of patients with rheumatoid arthritis. *J Chromatogr B Biomed Sci Appl* 1997; **688**:229–37.
  - 15 Rops AL, van den Hoven MJ, Bakker MA *et al.* Expression of glomerular heparan sulphate domains in murine and human lupus nephritis. *Nephrol Dial Transplant* 2007; **22**:1891–902.
  - 16 Chui D, Sellakumar G, Green R *et al.* Genetic remodeling of protein glycosylation *in vivo* induces autoimmune disease. *Proc Natl Acad Sci USA* 2001; **98**:1142–7.
  - 17 Green RS, Stone EL, Tenno M, Lehtonen E, Farquhar MG, Marth JD. Mammalian N-glycan branching protects against innate immune self-recognition and inflammation in autoimmune disease pathogenesis. *Immunity* 2007; **27**:308–20.
  - 18 Wada Y. Mass spectrometry in the detection and diagnosis of congenital disorders of glycosylation. *Eur J Mass Spectrom (Chichester, Eng)* 2007; **13**:101–3.
  - 19 Faid V, Chirat F, Seta N, Foulquier F, Morelle W. A rapid mass spectrometric strategy for the characterization of N- and O-glycan chains in the diagnosis of defects in glycan biosynthesis. *Proteomics* 2007; **7**:1800–13.
  - 20 Miyamoto S. Clinical applications of glycomic approaches for the detection of cancer and other diseases. *Curr Opin Mol Ther* 2006; **8**:507–13.
  - 21 Yuan J, Hashii N, Kawasaki N, Itoh S, Kawanishi T, Hayakawa T. Isotope tag method for quantitative analysis of carbohydrates by liquid chromatography-mass spectrometry. *J Chromatogr A* 2005; **1067**:145–52.
  - 22 Alvarez-Manilla G, Warren NL, Abney T, Atwood J III, Azadi P, York WS, Pierce M, Orlando R. Tools for glycomics: relative quantitation of glycans by isotopic permethylation using <sup>13</sup>CH<sub>3</sub>I. *Glycobiology* 2007; **17**:677–87.
  - 23 Kang P, Mechref Y, Kysekova Z, Goetz JA, Novotny MV. Comparative glycomic mapping through quantitative permethylation and stable-isotope labeling. *Anal Chem* 2007; **79**:6064–73.
  - 24 Bowman MJ, Zaia J. Tags for the stable isotopic labeling of carbohydrates and quantitative analysis by mass spectrometry. *Anal Chem* 2007; **79**:5777–84.
  - 25 Watanabe-Fukunaga R, Brannan CI, Copeland NG, Jenkins NA, Nagata S. Lymphoproliferation disorder in mice explained by defects in Fas antigen that mediates apoptosis. *Nature* 1992; **356**:314–7.
  - 26 Adachi M, Watanabe-Fukunaga R, Nagata S. Aberrant transcription caused by the insertion of an early transposable element in an intron of the Fas antigen gene of lpr mice. *Proc Natl Acad Sci USA* 1993; **90**:1756–60.
  - 27 Merino R, Iwamoto M, Fossati L, Izui S. Polyclonal B cell activation arises from different mechanisms in lupus-prone (NZB x NZW)<sub>F<sub>1</sub></sub> and MRL/MpJ-lpr/lpr mice. *J Immunol* 1993; **151**:6509–16.
  - 28 Homma H, Tozawa K, Yasui T, Itoh Y, Hayashi Y, Kohri K. Abnormal glycosylation of serum IgG in patients with IgA nephropathy. *Clin Exp Nephrol* 2006; **10**:180–5.
  - 29 Hase S, Okawa K, Ikenaka T. Identification of the trimannosylchitobiose structure in sugar moieties of Japanese quail ovomucoid. *J Biochem* 1982; **91**:735–7.
  - 30 Kubelka V, Altmann F, Kornfeld G, Marz L. Structures of the N-linked oligosaccharides of the membrane glycoproteins from three lepidopteran cell lines (Sf-21, IZD-Mb-0503, Bm-N). *Arch Biochem Biophys* 1994; **308**:148–57.
  - 31 Natsuka S, Adachi I, Kawaguchi M, Nakakita S, Hase S, Ichikawa A, Ikura K. Structural analysis of N-linked glycans in *Caenorhabditis elegans*. *J Biochem* 2002; **131**:807–13.
  - 32 Altmann F, Schwihla H, Staudacher E, Glossl J, Marz L. Insect cells contain an unusual, membrane-bound beta-N-acetylglucosaminidase probably involved in the processing of protein N-glycans. *J Biol Chem* 1995; **270**:17344–9.
  - 33 Guo S, Sato T, Shirane K, Furukawa K. Galactosylation of N-linked oligosaccharides by human beta-1,4-galactosyltransferases I, II, III, IV, V, and VI expressed in Sf-9 cells. *Glycobiology* 2001; **11**:813–20.
  - 34 Jeddi PA, Lund T, Bodman KB *et al.* Reduced galactosyltransferase mRNA levels are associated with the agalactosyl IgG found in arthritis-prone MRL-lpr/lpr strain mice. *Immunology* 1994; **83**:484–8.
  - 35 Cameron JS. Lupus nephritis. *J Am Soc Nephrol* 1999; **10**:413–24.
  - 36 Walport MJ. Complement. First of two parts. *N Engl J Med* 2001; **344**:1058–66.
  - 37 Walport MJ. Complement. Second of two parts. *N Engl J Med* 2001; **344**:1140–4.
  - 38 Botto M. Links between complement deficiency and apoptosis. *Arthritis Res* 2001; **3**:207–10.
  - 39 Hanayama R, Tanaka M, Miyasaka K, Aozasa K, Koike M, Uchiyama Y, Nagata S. Autoimmune disease and impaired uptake of apoptotic cells in MFG-E8-deficient mice. *Science* 2004; **304**:1147–50.
  - 40 Arason GJ, Steinsson K, Kolka R, Vikingsdottir T, D'Ambrogio MS, Valdimarsson H. Patients with systemic lupus erythematosus are deficient in complement-dependent prevention of immune precipitation. *Rheumatology (Oxford)* 2004; **43**:783–9.
  - 41 Cook HT, Botto M. Mechanisms of disease: the complement system and the pathogenesis of systemic lupus erythematosus. *Nat Clin Pract Rheumatol* 2006; **2**:330–7.
  - 42 Gunnarsson I, Sundelin B, Heimburger M, Forslid J, van Vollenhoven R, Lundberg I, Jacobson SH. Repeated renal biopsy in proliferative lupus nephritis – predictive role of serum C1q and albuminuria. *J Rheumatol* 2002; **29**:693–9.
  - 43 Buyon JP, Tamerius J, Belmont HM, Abramson SB. Assessment of disease activity and impending flare in patients with systemic lupus erythematosus. Comparison of the use of complement split products and conventional measurements of complement. *Arthritis Rheum* 1992; **35**:1028–37.
  - 44 Markiewski MM, Lambris JD. The role of complement in inflammatory diseases from behind the scenes into the spotlight. *Am J Pathol* 2007; **171**:715–27.
  - 45 Sturfelt G. The complement system in systemic lupus erythematosus. *Scand J Rheumatol* 2002; **31**:129–32.
  - 46 Holmskov U, Malhotra R, Sim RB, Jensenius JC. Collectins: collagenous C-type lectins of the innate immune defense system. *Immunol Today* 1994; **15**:67–74.

## Differential analysis of N-glycan in the kidney in a SLE mouse model

- 47 Weis WI, Drickamer K, Hendrickson WA. Structure of a C-type mannose-binding protein complexed with an oligosaccharide. *Nature* 1992; **360**:127–34.
- 48 Takahashi M, Mori S, Shigeta S, Fujita T. Role of MBL-associated serine protease (MASP) on activation of the lectin complement pathway. *Acta Exp Med Biol* 2007; **598**:93–104.
- 49 Turner MW. Mannose-binding lectin: the pluripotent molecule of the innate immune system. *Immunol Today* 1996; **17**:532–40.
- 50 Holmskov U, Malhotra R, Sim RB, Jensenius JC. Collectins: collagenous C-type lectins of the innate immune defense system. *Immunol Today* 1994; **15**:67–74.
- 51 Thiel S, Vorup-Jensen T, Stover CM *et al.* A second serine protease associated with mannan-binding lectin that activates complement. *Nature* 1997; **386**:506–10.
- 52 Lhotia K, Wurznier R, König P. Glomerular deposition of mannose-binding lectin in human glomerulonephritis. *Nephrol Dial Transplant* 1999; **14**:881–6.
- 53 Ohsawa I, Ohi H, Tamano M *et al.* Cryoprecipitate of patients with cryoglobulinemic glomerulonephritis contains molecules of the lectin complement pathway. *Clin Immunol* 2001; **101**:59–66.
- 54 Trouw LA, Seelen MA, Duijjs IM *et al.* Activation of the lectin pathway in murine lupus nephritis. *Mol Immunol* 2005; **42**:731–40.
- 55 Jorgensen TN, Gubbels MR, Kotzin BL. New insights into disease pathogenesis from mouse lupus genetics. *Curr Opin Immunol* 2004; **16**:787–93.
- 56 Lauwerys BR, Wakeland EK. Genetics of lupus nephritis. *Lupus* 2005; **14**:2–12.

## Gene Expression Profiling of Human Mesenchymal Stem Cells for Identification of Novel Markers in Early- and Late-Stage Cell Culture

Shihori Tanabe\*, Yoji Sato, Takayoshi Suzuki, Kazuhiro Suzuki, Taku Nagao and Teruhide Yamaguchi\*

Division of Cellular and Gene Therapy Products, National Institute of Health Sciences, Tokyo 158-8501, Japan

Received January 9, 2008; accepted June 5, 2008; published online June 11, 2008

Human mesenchymal stem cells (hMSCs) are multipotent cells that differentiate into several cell types, and are expected to be a useful tool for cellular therapy. Although the hMSCs differentiate into osteogenic cells during early to middle stages, this differentiation capacity decreases during the late stages of cell culture. To test a hypothesis that there are biomarkers indicating the differentiation potential of hMSCs, we performed microarray analyses and profiled the gene expression in six batches of hMSCs (passages 4–28). At least four genes [necdin homolog (mouse) (NDN), EPH receptor A5 (EPHA5), nephroblastoma overexpressed gene (NOV) and runt-related transcription factor 2 (RUNX2)] were identified correlating with the passage numbers in all six batches. The results showed that the osteogenic differentiation capacity of hMSCs is down-regulated in the late stages of cell culture. It seemed that adipogenic differentiation capacity was also down-regulated in late stage of the culture. The cells in late stage are oligopotent and the genes identified in this study have the potential to act as quality-control markers of the osteogenic differentiation capacity of hMSCs.

**Key words:** cellular therapy, culture stage marker, differentiation, gene expression, stem cell.

Abbreviations: EPHA5, EPH receptor A5; hMSCs, human mesenchymal stem cells; NDN, necdin homolog (mouse); NOV, nephroblastoma overexpressed gene; PBS, phosphate buffered saline; RUNX2, runt-related transcription factor 2.

### INTRODUCTION

'Cellular therapy' is a new concept in treating diseases with cells that have regeneration potential. Currently, it is at the clinical research stage; however, the use of cellular therapeutics in regular clinical settings will be implemented in near future. Cellular therapeutics involves the use of cells derived from human tissue, either cultured and/or modified, in regenerating and repairing damaged tissues and consequently improving the functions in the human body. Hence, tissue or embryonic stem cells that have the potential to differentiate into a variety of cell types are one of the prime candidate cells for cellular therapeutics. It is difficult to overview the entire discipline of cellular therapeutics since the cells themselves represent 'life'.

Stem cells, one of the candidates for cellular therapeutics, produce daughter cells identical to themselves that differentiate into other types of cells (1). The fate of the stem cells is determined by cellular signaling, although the underlying mechanism is still unknown.

It is therefore important to investigate the gene expression patterns that influence the cellular signaling pathways and identify the representative biomarkers that can act as indicators of the differentiation potential of the stem cells. Recently, it has been reported that human somatic cells can be induced to pluripotent stem cells (2).

There have been several reports suggesting that cellular therapeutics is a promising treatment for several diseases. C-kit-expressing cells obtained from the bone marrow have been used in cardiac tissue repair in mice experiments (3). Previous studies have reported the use of autologous bone marrow cells transplantation for the post-infarction recovery of cardiac function (4–9). Cytotoxic T cells have also been used for cellular therapy to protect from infectious diseases in an immunodeficient condition following hematopoietic stem cell transplantation (10). Mesenchymal stem cells (MSCs) are also used for therapy expecting immunosuppressive effects (11, 12). Previous studies on MSCs also indicate that these cells possess the ability for chondrogenic (13), osteogenic (14, 15) and adipogenic differentiation, and possibly other differentiating capabilities (16). In a clinical setting, it is difficult to assess the overall profile of each batch of the cells. We hypothesized the existence of quality-control markers for the differentiation potential of human mesenchymal stem cells (hMSCs) and used gene expression profiling to identify these markers.

\*To whom correspondence should be addressed. Tel: +81-3-3700-1141, Fax: +81-3-3700-9217, E-mail: stanabe@nihs.go.jp

\*Present address: Division of Biological Chemistry and Biologicals, National Institute of Health Sciences

## EXPERIMENTAL PROCEDURES

**Cell Culture**—The hMSCs derived from bone marrow [Lonza (Cambrex), Walkersville, Maryland, USA] were cultured in mesenchymal stem cell growth medium (MSCGM) [Lonza (Cambrex) #PT-3001; mesenchymal stem cell basal medium supplemented with mesenchymal cell growth supplement, L-glutamine and penicillin/streptomycin] at 37°C in CO<sub>2</sub> (5%) incubator. Cells were passaged according to the manufacturer's protocol with slight modification using trypsin-EDTA solution [Lonza (Cambrex) #CC-3232]. Lot numbers of the hMSC batches were as follows: #4F1127, #4F0312, #5F0138, #4F1560, #4F0591 and #4F0760. Informed consent was obtained in Poietics human mesenchymal stem cell systems [Lonza (Cambrex)]. All differentiation procedures were performed according to Lonza (Cambrex) protocol with slight modification.

**Osteogenic Differentiation**—The hMSCs were plated onto 12-well plates and 24 h later, the medium was changed to MSCGM (as control) or osteogenic induction medium (OIM) [Lonza (Cambrex) #PT-3002; differentiation basal medium containing dexamethasone, ascorbate, mesenchymal cell growth supplement, L-glutamine, penicillin/streptomycin and  $\beta$ -glycerophosphate]. Medium was changed every 3–4 days and cells were differentiated for 21 days.

**Calcium Deposition Assay**—Calcium deposition was measured using the Stanbio Total Calcium Liquicolor<sup>®</sup> kit (Stanbio Laboratory, Boerne, Texas, USA; #0150-250) according to the manufacturer's protocol (Cambrex, Stanbio Laboratory). Briefly, the cells cultured on 12-well plates for 22 days (osteogenic-induced for 21 days) were rinsed with phosphate buffered saline (PBS) without calcium and magnesium [Lonza (Cambrex) #17-516Q] and harvested in 0.5 N HCl (600  $\mu$ l). Calcium was extracted from the cells by shaking the tubes for approximately 20 h at 4°C. Lysates were centrifuged at 500g for 2 min at 4°C and 20  $\mu$ l of the supernatant was used for the assay. Absorption at 560 nm was measured to detect the Ca-ortho-cresolphthalein complexone (OCPC) complex using an EnVision 2103 multilabel reader (PerkinElmer, Waltham, Massachusetts, USA). Calcium deposition was adjusted with the total protein concentration of the samples. Cells harvested in 0.5 N HCl were centrifuged at 15,000 rpm for 10 min at 4°C. The pellet was washed once with PBS without calcium and magnesium, and resuspended in 100  $\mu$ l of 0.1 N NaOH/0.1% SDS. After overnight incubation at 37°C, the lysate was centrifuged at 15,000 rpm for 10 min at room temperature, and the supernatant was quantitated using the DC protein assay (Bio-Rad Laboratories, Hercules, California, USA) according to the manufacturer's protocol. Absorbance at 620 nm was measured using the EnVision 2103 multilabel reader (PerkinElmer). The standard curve was obtained using bovine serum albumin.

**Adipogenic Differentiation**—The cells were plated onto a 24 well-plate at  $2.1 \times 10^4$ /cm<sup>2</sup>, and cultured in MSCGM for 5–6 days. After cells reach confluence, medium was changed to MSCGM (as control) or adipogenic induction medium (AIM) [Lonza (Cambrex) #PT-3004; induction basal medium supplemented with recombinant human

insulin, L-glutamine, mesenchymal stem cell growth supplement, penicillin/streptomycin, dexamethasone, indomethacin and IBMX (3-Isobutyl-1-methylxanthine)]. Medium was changed after 3 days into adipogenic maintenance medium (maintenance basal medium supplemented with recombinant human insulin, L-glutamine, penicillin/streptomycin and mesenchymal stem cell growth supplement). After three complete cycles of induction/maintenance, the cells were cultured for 7 more days in adipogenic maintenance medium, replacing the medium every 2–3 days.

**Oil Red O staining**—The cells were rinsed with 500  $\mu$ l of PBS and fixed with 10% neutral buffered formalin (500  $\mu$ l). After washing with sterile water, the cells were washed with 60% 2-propanol (500  $\mu$ l) for 2–5 min and stained with Oil Red O (500  $\mu$ l) for 5 min. The cells were rinsed with tap water and stained with Harris' haematoxylin (500  $\mu$ l) for 1 min and rinsed with the water. Lipid vesicles were observed with microscope Biozero BZ-8000 (KEYENCE, Osaka, Japan).

**Chondrogenic Differentiation**—The cells ( $3 \times 10^5$ ) were washed with incomplete chondrogenic induction medium [Lonza (Cambrex) #PT-3003; chondrogenic basal medium containing dexamethasone, ascorbate, ITS (insulin-transferrin-sodium selenite) + supplement, sodium pyruvate, proline, penicillin/streptomycin, L-glutamine] and were resuspended in 0.5 ml of complete chondrogenic induction medium (CCIM; incomplete chondrogenic induction medium supplemented with 10 ng/ml of TGF- $\beta$ 3) or MSCGM (as control) and cultured in 15 ml polypropylene culture tubes. The medium was replaced every 3–4 days and the cells were cultured for 24 days.

**Safranin-O Stains for in vitro Chondrogenesis**—The chondrogenic pellets were fixed in 10% neutral buffered formalin and paraffin embedded. The paraffin sections were stained with Weigert's iron hematoxylin (Wako 298-21741), 0.02% fast green FCF (MP biomedical 195178) and 0.1% Safranin-O (Sigma HT 90432), followed by observation with microscope Biozero BZ-8000 (KEYENCE).

**Total RNA Purification**—The hMSCs were cultured on a 10 cm dish, lysed in 600  $\mu$ l of Buffer RLT (RNeasy<sup>®</sup> Lysis Buffer) with  $\beta$ -mercaptoethanol and homogenized using a QIA shredder (QIAGEN, Düsseldorf, Germany). Total RNA was purified using RNeasy<sup>®</sup> mini spin columns according to manufacturer's protocol (QIAGEN). Total RNA was eluted with RNase-free water.

**Microarray Analysis**—Total RNA (100 ng or 1  $\mu$ g) was reverse transcribed and amplified using a GeneChip<sup>®</sup> kit (Affymetrix, Santa Clara, California, USA) and the biotinylated cRNA was hybridized onto the GeneChip<sup>®</sup> Human Genome U133 Plus 2.0 Array (54,613 probe sets). The data was analysed using GeneChip Operating System software (versions 1.2–1.4), followed by statistical analysis. The data was also analysed using GeneSpring<sup>™</sup> (version 7.3) (Agilent, Santa Clara, California, USA). The data discussed in this publication have been deposited in NCBI's Gene Expression Omnibus (GEO; <http://www.ncbi.nlm.nih.gov/geo/>) (17, 18). They are accessible through GEO Series accession number GSE7637 for the data from 4F1560, and GSE7888 for the data obtained from all six batches. The statistical method for microarray data analysis has been also discussed elsewhere (19).

**Cluster Analysis**—The microarray data of 169 probe sets obtained from six batches of hMSCs was subject to cluster analysis using the Gene Expression Statistical System (NCSS, Kaysville, Utah; Dr Jerry L. Hintze). Fold change of signal intensity to the average signal intensity of early stage was analysed and a double dendrogram was plotted on a log 2 scale.

**Gene Ontology Analysis**—Gene ontology analysis was conducted using Ingenuity Pathway Analysis (IPA) (Ingenuity<sup>®</sup> Systems, Redwood City, California, USA), NetAffyx (Affymetrix) and GOTM (Gene Ontology Tree Machine, Vanderbilt University, Nashville, Tennessee, USA) analyses. Probe sets with signal intensity values associated with the passage numbers were subject to analyses. The functional analysis identified the biological function and/or diseases that were most significant to the data set. Genes from the data set that were associated with biological functions and/or diseases in the Ingenuity Pathways Knowledge Base (IPKB) were considered for further analysis.

**cDNA Synthesis and Real-time PCR Using Taqman Low-density Array**—RT-PCR (reverse transcriptase-PCR) analysis was performed to assess the mRNA levels in six batches of hMSCs using TaqMan<sup>®</sup> low-density array (TLDA) (Format 48) (Applied Biosystems, Foster City, California, USA). The data was normalized using GAPDH (glyceraldehyde-3-phosphate dehydrogenase). Forty-six genes including GAPDH as endogenous control are listed in Supplementary Table 1. cDNA was synthesized using a High-capacity cDNA synthesis kit (Applied Biosystems) and Multiscribe reverse transcriptase. cDNA synthesized from 100 ng of total RNA was used for the analysis (2 ng of total RNA per well). Real-time PCR was analysed using 7900 HT real-time PCR system (Applied Biosystems). The conditions for the PCR reaction were as follows: 50°C (2 min) and 94.5°C (10 min), and 40 cycles at 97°C (30 sec) and 59.7°C (1 min). Relative quantification values were calculated by the comparative Ct method using SDS 2.2.2 software (Applied Biosystems).

**Pathway Network Analysis**—Data were analysed using the IPA (Ingenuity<sup>®</sup> Systems, www.ingenuity.com). A data set containing gene identifiers and corresponding expression values was uploaded into the application. Each gene identifier was mapped to its corresponding gene object in the IPKB. A fold-change cutoff of 3 for both up- and down-regulation and a *p*-value cutoff of 0.05 were set to identify the genes to be analysed. These genes, called focus molecules, were overlaid onto a global molecular network developed from information in the IPKB. Networks of these focus molecules were then algorithmically generated based on their connectivity. The functional analysis of a network identified the biological functions and/or diseases that were most significant to the genes in the network. The genes in the networks associated with biological functions and/or diseases in the IPKB were considered for the analysis. Genes and gene products are represented as nodes, and the biological relationship between two nodes is represented as an edge (line). All edges are supported by at least one reference from the literature, textbook or canonical information stored in the IPKB. Human, mouse and rat orthologs of a gene are stored as separate

objects in the IPKB, but are represented as a single node in the network. The node colour indicates the degree of up- (red) or down- (green) regulation. Nodes are displayed using various shapes that represent the functional class of the gene product.

**Statistical Analyses**—Non-parametric analysis was used for microarray data analyses. The Spearman correlation coefficient and two-tailed *p*-values were calculated. *P* < 0.001 or *P* < 0.05 were considered to be significant. RT-PCR data was analysed with non-parametric analysis. The Spearman correlation coefficient and two-tailed *p*-values were calculated. To compare the specific passage number and stage, Student's *t* test was performed. Two-way ANOVA followed by Bonferroni post-test was performed for osteogenesis data. GraphPad Prism<sup>®</sup> 4 and Microsoft<sup>®</sup> Office Excel were used for statistical analysis and drawing graphs.

## RESULTS

**Microarray Analysis of hMSCs**—To identify the quality-control markers in different stage of the culture, we performed DNA microarray analyses. Non-parametric analysis and a ratio (max/min of signal intensity) cutoff of 3.071,524 ( $1.05^{28-5}$ ; 5% change in each passage from 5th to 28th) showed that the expression level of 341 probe sets out of a total of 54,613 probe sets had a significant association with passage numbers (hMSC lot #4F1560, passage numbers 5, 7, 9, 13, 21 and 28).

Gene ontology analyses showed that the mapped genes corresponded to the probe sets belonging to various categories of molecular and cellular functions such as cell-to-cell signaling and interaction, cellular movement, cell death, cellular assembly, cellular organization and cell cycle, and physiological system development, and biological functions such as hematological system development and function, immune and lymphatic system development and function, tissue development, immune response and embryonic development. The top five disease categories that the genes mapped to, as identified using the IPA software, included cardiovascular, hematological, musculoskeletal, oncogenic and reproductive disorders.

Figure 1 shows the results of cluster analysis obtained from microarray data of six batches of hMSCs in early (passage #4–5), middle (#7–9) and late stages (#22–28). Seventy-nine genes out of the 169 probe sets were categorized by function and disease as per IPA analysis. Networks were analysed for each of the six batches and a representative network is shown in the Supplementary Fig. 1. A list of all top networks in each analysis is shown in Table 1. Many network categories with the top score in each analysis were involved in cancer or regulation of cell cycle. Additionally, specific networks for each sample were generated when the batches were individually analysed.

**Calcium Deposition of Osteogenic-induced Cells**—In Fig. 2, calcium deposition in hMSC cultures (4F0312, 5F0138, 4F1560, 4F0591, 4F0760) were measured during passages 7, 9, 10 and 19. The results showed that the osteogenic differentiation occurred in early to middle stages and was dramatically suppressed during the late

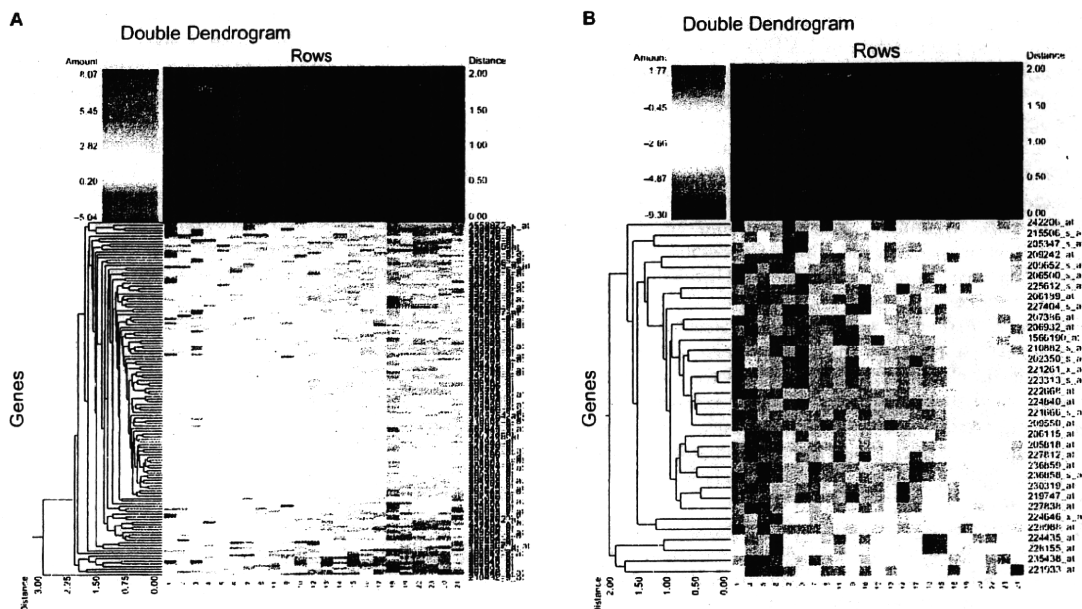


Fig. 1. Microarray analysis of hMSCs. One hundred and sixty-nine probe sets extracted from microarray data of six batches of hMSCs. [ $n=6$  in early stage (#4 or 5), passage #9, late stage (#22, 24 or 28),  $n=5$  in passage #7]. Cut off value of signal intensity ratio (max/min of average in each stage) is

2.949145023 [5% change in each passage number from early to late stage; 1.05 (passage number range of average in early and late stage)]. Double dendrograms of up-regulated 135 probe sets (A) and down-regulated 34 probe sets (B) are shown.

stages of cell culture. These findings suggest that the expression levels of genes associated with osteogenesis are different at the late stages compared with those at earlier stages of cell culture.

Statistical analysis of microarray and calcium deposition data from three batches (5F0138, 4F1560, 4F0591) of hMSCs in middle (#7–10) and late (#19–28) stages showed that the expression of *NDN* (necdin homolog (mouse)) has a positive correlation with calcium deposition ( $P < 0.05$ ).

**Adipogenic Differentiation of hMSCs**—Figure 3A shows the results of Oil Red O staining of adipogenic-induced cells. The cells were adipogenic induced for 21 days and lipid was stained with Oil Red O. Adipogenesis of hMSCs seemed to be down-regulated in late culture stage of 5F0138, 4F0591 and 4F0760, while the adipogenic-differentiation capacity seemed to be retained in passage #20 of 4F1560.

**Chondrogenic Differentiation of hMSCs**—Figure 3B shows the Safranin-O staining of chondrogenic-differentiated hMSCs. The cells were differentiated in CCIM for 24 days and stained with Safranin-O. The culture in passages 7, 17 and 22 of 4F0591 showed chondrogenic-differentiated morphology (a, b, c, respectively). The culture in late stage seemed to be chondrogenic differentiated as shown (c). The cells cultured in MSCGM as control did not show any chondrogenic-differentiated morphology (d).

**RT-PCR Analysis of hMSCs**—The quantitative RT-PCR data showed that some genes had similar expression profiles in all the six batches examined. Up-regulated genes, which were identified as candidates

for the stage-specific markers included *EPHA5* (EPH receptor A5), *NOV* (nephroblastoma overexpressed gene), *SERPINE1* [serpin peptidase inhibitor clade E (nexin, plasminogen activator inhibitor type 1), member 1], *ITGA4* [integrin, alpha 4 (antigen CD49D, alpha 4 subunit of VLA-4 receptor)], and down-regulated genes, which are also candidates for the stage-specific markers included *NDN*, *RUNX2* (runt-related transcription factor 2) and *RUNX3* (runt-related transcription factor 3). *NOV* is a growth factor and is involved in the proliferation of bone cancer cell lines (20). It is notable that the expression of *NOV* in lot #4F1127 was relatively stable. *SERPINE1* is involved in the protein-binding function and diseases such as heart failure (21). *RUNX2* is a member of the runt domain-containing family of transcription factors and suggested to regulate osteogenic differentiation (22). *RUNX3* is also a member of the runt domain-containing family of transcription factors and a candidate tumor suppressor (23). *EPHA5*, *NOV*, *NDN* and *RUNX2* showed altered expression correlating with passage numbers ( $P < 0.01$ ) (Fig. 4). The results of RT-PCR analysis of 45 genes examined are shown in Supplementary Fig. 2.

## DISCUSSION

hMSCs will be used for cellular therapeutics in clinical settings in the near future. The importance of quality control of the cells will be significant as the use of cellular therapeutics becomes more common. In this report, we report on profiling the gene expression of

Table 1. List of the networks in hMSCs.

Analysis	Molecules in network	Score	Focus molecules	Top functions
4F0591-#9	PUB1B, CCNB1, CDC2, CDKN3, CENPF, CGRRF1, Cyclin E, DJG7, E2f, ERCC6L, FOXM1, KRT8, LRP1, MAD2L1, MEOX2, NDC80, NFKB, NUF2, NUSAP1, OLR1, PBK, PCSK1, PLK1, PTTG1, RAD51AP1, Rb, RNA polymerase II, RRM2, SERPINB2, SPC25, TFP12, TNFSF9, TRADD, TYMS, UBE2C	65	30	Cell Cycle, Cancer, Reproductive System Disease
4F1560-#28	ADH1B, ALDH1A3, BEX1 (includes EG:55859), BMP15, CD80, CHI3L1, DBP, DLX1, ENPP1, FGF5, GBP2, IGF2, Igfbp, IGFBP5, KRT19, LBP, MEOX2, Mmp, NFKB, NOV, PCSK1, PCSK5, PEG10, PYCARD, RAGE, SEPP1, SERPINB2, SERPING1, ST8SIA1, Tgf beta, TLR1, TNFAIP6, TNFSF15, TRAF4, TSLP	57	31	Cancer, Cellular Growth and Proliferation, Neurological Disease
4F0760-#9	ANKRD1, Ap1, BIRC3, CCNB1, CCR2, CDC2, CENPE, COL15A1, FBLN5, Jnk, LAT51, Mmp, MSRI, NDC80, NFKB, NRL, NUF2, OMD, PBK, PdGf, PDGF BB, PDGFD, PRDM1, S100A4, SERPINB2, SLC37A4, SORBS3, SPC24, SPC25, TFP12, THBD, TNFRSF8, VANGL2, VAV3, VSNL1	56	29	Cancer, Cell Cycle, Reproductive System Disease
5F0138-#24	ARI4C, RUI1 (includes EG:699), BUB1B, CCNB1, CCNB2, CCNF, CDC2, CDC7, CDC20, CDC25C, CDKN3, CENPE, CENPH, Cyclin B, Cyclin E, FEXO5, FOXM1, GINS1, GPNMB, IL6, KIAA0101, KIF11, KIF22, KIF2C, MRV1, NDC80, NUF2, PBK, PLK4, PTTG1, SLC7A7, SPC25, UBE2C, VTCN1, ZWINT (includes EG:11130)	52	33	Cell Cycle, Cancer, DNA Replication, Recombination, and Repair
4F1560-#9	14-3-3, AURKA, BIRC5, CCNB1, CDC20, CDC25C, CDCA8, Cyclin B, Cyclin E, E2f, IGF2, MAD2L1, NDC80, NFKB, NUF2, OLR1, PBK, PRR11, RAD51AP1, Rb, RGS7, RNA polymerase II, RRM2, Sef, SERPINB2, SFN, SFRP4, SPC24, SPC25, TNFRSF8, TOP2A, TYMS, UBE2C, UHRF1, ZNF74	52	27	Cancer, Cell Cycle, Reproductive System Disease
4F0591-#28	AEBP1, ALDH1A3, ANGPT1, ANKRD1, BEX1 (includes EG:55859), CIR, CGREF1, CXCL16, DIRAS3, GADI, HDAC9, ID4, IL1, IL1R1, KRT18, KRT19, MEOX2, Mmp, MYBL1, MYFN, NFKB, OLR1, PAK1IP1, PdGf Ab, PLAT, PYCARD, RIFK4, SERPINB2, SERPINF1, SERPING1, TFP12, Tgf beta, TNFRSF19, TNFRSF11B, TSLP	51	30	Cancer, Cardiovascular Disease, Cell Death
4F0312-#7	A2M, ACAN, ASPN, BRCA1, CIR, C1S, CEBPD, CYP27A1, DDIT3, DDIT4, ESRI, FGF7, GDF15, IL1, Jnk, KSR2, MAD2L1, Mek, Mek1/2, Mmp, NFKB, NOTCH3, NOX4, NR4A1, OSMR, P38 MAPK, PCK2, PdGf, PDGF BB, SERPINB2, STAT, TNFAIP6, TNFSF9, TNFSF15, TRIB3	50	25	Cell Cycle, Inflammatory Disease, Cellular Development
4F0312-#28	ANKRD1, BEX1 (includes EG:55859), BLK, CD36, CDKN2B, CTSL2, ENPP1, F2RL1, FABP5, FKBP5, FUS, GOS2, GAD1, GDF15, IGFBP5, IGHG1, IL1, N-cor, NFKB, OLR1, PAPP2, PLAT, PNR1, Rxr, RXRA, SERPINB2, STMN2, Tgf beta, THR, Thyroid hormone receptor, TNFRSF19, TNFRSF11B, TNFSF13B, TRIP13, VSNL1	50	29	Cancer, Cellular Growth and Proliferation, Immunological Disease
4F1560-#7	14-3-3, AURKA, BIRC5, CCNE2 (includes EG:9134), CDC25A, CDCA8, CEBPA, CENPF, CSPG4, Cyclin A, Cyclin E, E2f, ESPL1, FEN1, FMO5, Histone h3, Mapk, MCM8, MCM10, MDM4, NUSAP1, OIP5, PP2A, PRR11, PTTG1, Rb, RGS7, RRM2, SFRP4, SMPDL3A, SOS2, TOP2A, TTK, TYMS, UBE2C	50	27	Cell Cycle, Cancer, Reproductive System Disease
4F0312-#9	ACAN, AEBP1, Akt, ANXA11, ASPN, CIR, C1S, CD36, DKK, F2RL1, FBLN1, FGF7, FOXE1, GDA, GDF15, HSD11B1, IGF2, IGFBP2, Insulin, LDL, LEPR, Mapk, NFKB, NTF3, P38 MAPK, PDGF BB, PTX3, SLC7A7, THBS2, TNFAIP6, TNFSF9, Wnt, WNT2, WNT16	49	23	Lipid Metabolism, Molecular Transport, Small Molecule Biochemistry

(continued)



Table 1. Continued.

Analysis	Molecules in network	Score	Focus molecules	Top functions
5F0138-#9	ABCA1, AEBP1, ARG2, BGN, C1q, CIR, CIS, CYP2B6 (includes EG:1555), DDIT4, ENPP1, FABP5, FADS1, GDF15, HABP2, N-cor, NCOR-LXR-Oxysterol-RXR-9 cis RA, NFKB, Nr1h, OLR1, PCK2, PDGF BB, PTGDR, Rxr, SCD, SERPING1, SFTPD, SORBS3, SREBF1, SYNE1, THBS2, Thyroid hormone receptor, TNFAIP6, TNFSF9, TRIB3, VDR	46	27	Respiratory Disease, Inflammatory Disease, Lipid Metabolism
4F1127-#9	ACAN, Alkaline Phosphatase, Api, ASPN, C3, CCL2, CCNO, COL13A1, CP, FABP5, GEM, HMOX1, HOMER2, IGFBP5, IL1, JAG1, LDB3, LDL, Mmp, MMP28, NFKB, P38 MAPK, Pdgf, PDGF BB, RGS4, SERPINB2, SPINT2, SPPI, TAC1, Tgf beta, TNFAIP6, TNFRSF11B, TXNIP, VitaminD3-VDR-RXR, ZNF335	45	24	Cellular Development, Cellular Growth and Proliferation, Skeletal and Muscular System Development and Function
4F1127-#22	AEBP1, ANKRD1, C1q, C1r, CBR3, CD36, CFH, ENPP1, FLNC, FOXF1, GOS2, HAMP, HDL, HIST2H2AA3, HIST2H2BE, HIVEP1, IGKC, KCNAB1, KCND2, KRT17, LDB3, LY6E (includes EG:4061), MYOZ1, NFKB, OLR1, PIK3, POU2F2, REG3A, RIPK4, SLC40A1, TNFRSF19, TNFRSF10D, TNFSF9, TSLP, VSNL1	44	32	Genetic Disorder, Metabolic Disease, Molecular Transport
4F0760-#28	Alpha Actinin, CDH1, CTSH, Cyclin A, Cyclin E, Ezr, EDN1, GAST, ICAM2, Integrin, ITGA2, ITGA6, KRT7, KRT18, LAMC2, MARCKSL1, Mek1/2, Mmp, MYO22, OCLN, PCOLCE, PCOLCE2, Plc beta, PLCB4, PRPS1, Rb, S100A4, SCG5, SDPR, SERPINB2, SMURF2, TFP2, TGFB1, TNFRSF11B, TSPAN8	44	26	Cardiovascular System Development and Function, Cell Morphology, Skeletal and Muscular System Development and Function
4F0591-#7	AMELX, AQP4, ARNT2, BAT3, beta-estradiol, BIRC5, CATSPERB, CDCA8, CEBPA, CGREF1, DLGAP1, GLIPR1, GPR37, GRIN1, GTSE1, HSPA2, HSPA5, INSI, LITAF, NCAPG (includes EG:64151), NFKB, NPAS1, PLGLB2, RAB31, RAGE, retinoic acid, RPS14, RPS4X, RRM2, SGG2, STXBP4, TF, TGFB1, TP53, TRHDE	38	16	Cell Death, Cancer, Respiratory Disease
4F1127-#7	Actin, ADIPOQ, Akt, Ap1, BCL9, BIRC5, CCL2, CPE, FGR2, ERCC6L, HIST1H4C, Histone h3, HOMER2, IL1, IL8, Jnk, KRT18, LDL, NFKB, OSBP, P38 MAPK, PBK, PDGF BB, PDGFC, PIK1, POSTN, PRDX4, SERPINA3, SFRP4, SLC2A3, Tgf beta, TIFA, TNFRSF11B, TNFRSF1B, TPST1	35	17	Cellular Growth and Proliferation, Cellular Development, Hematological System Development and Function
5F0138-#7	Akt, Ap1, ASNS, CALM2, DAD1, DDIT4, FSTL1, GOS2, GARS, GDF15, HTRA1, JAK3, LDHA, LDL, LOX, MMP1 (includes EG:4312), NFKB, P38 MAPK, PCK2, PCOLCE, PDGF BB, PDGFC, PDPN, RND3, REN2, SFRP1, SLC7A1, TOR, TGFB1, TIMP4, TNFRSF8, TNFSF9, TRIB3, UGDH, WNT2	30	15	Cancer, Cellular Movement, Cellular Development

The top networks in each analysis data analyzed by IPA are listed.

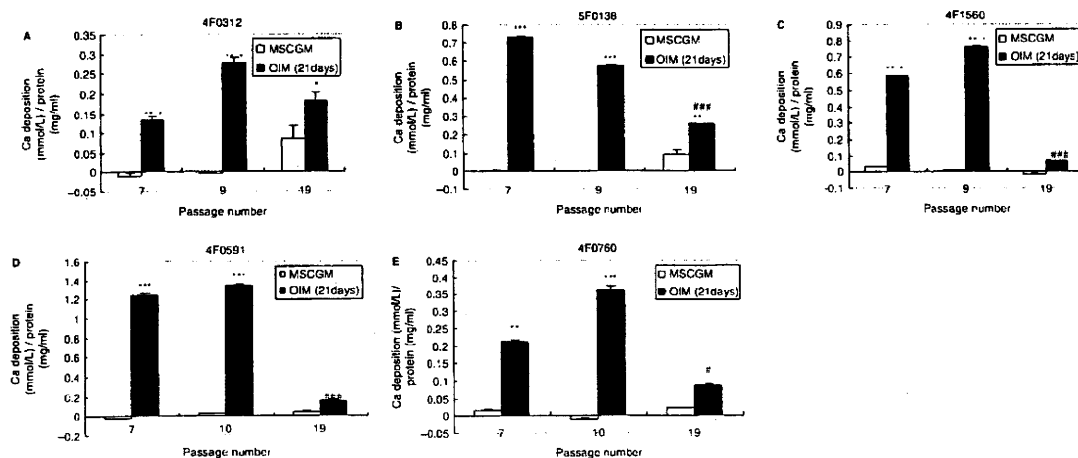


Fig. 2. Calcium deposition of hMSCs. The cells in each passage numbers indicated were plated on 12-well plates and cultured in MSCGM (control; clear column) or OIM (osteogenic differentiated; filled column) for 21 days. The amounts of calcium deposition in 4F0312, 5F0138, 4F1560, 4F0591 and 4F0760 are indicated in (A, B, C, D and E), respectively. Calcium deposition

divided by protein concentration is shown as mean + SEM in triplicate. \*\*\* $P < 0.001$ , \*\* $P < 0.01$ , \* $P < 0.05$  when osteogenesis in MSCGM was compared to that in OIM in each passage number. ###  $P < 0.001$ , ##  $P < 0.01$ , #  $P < 0.05$  when osteogenesis in passage #19 was compared to that in passage number 7 ( $n = 3$ ).

hMSCs through early and late stages of cell culture. Replication was performed by testing six different batches of cells. All six batches examined showed a marked decrease in culture growth rate with increasing passages.

The hMSC potential for osteogenic differentiation was down-regulated in all the batches of hMSCs examined during the late culture stage. The osteogenic differentiation was observed in all the batches of hMSCs examined for passages 7, 9 and 10. Also, every batch examined showed a down-regulation of the osteogenic process during the 19th passage. As previously stated, four genes, *NDN*, *EPHA5*, *NOV* and *RUNX2* showed altered expression depending on the culture stage. *EPHA5* and *NOV* were up-regulated as the cells were further passaged, while *NDN* and *RUNX2* were down-regulated.

RT-PCR data indicated that the expression of *NDN* in all batches examined decreased during the late stages of culture. The expression of *NDN* in lot #4F1127, #4F0312 and #5F0138 was relatively stable until the 14th passage, which was then followed by a decrease in expression during the late stages. Microarray data also showed that the expression of *NDN* in passages 22–28 were decreased compared to that in passages 4–8. Furthermore, our results showed a positive correlation between the expression of *NDN* in hMSCs and the potential to differentiate into osteogenic cells as measured by the calcium deposition rates. Previous reports suggested that neudin, an *NDN* homolog, interacts with IL-1 $\alpha$  precursor (24). The expression of *NDN* in hMSCs decreases with increasing passages. It is possible that *NDN* down-regulation is involved in activation of IL1-Myd88 pathway by dying cells (25).

Every batch showed a passage-dependent increase in the expression level of *EPHA5*. *EPHA5* is transmembrane receptor protein tyrosine kinase, known as Ephrin

A5 receptor, and belongs to the ephrin receptor subfamily. Recently, it has been shown that *EPHA5* is involved in cellular growth and tumor malignancies (26, 27). Also, it is known that the expression level of human *EPHA5* mRNA is high in primary human breast carcinoma cells (28).

*NOV/CCN3* is a growth factor that plays several roles in cellular migration, growth, proliferation and chemotaxis. The previous finding that *NOV* inhibits the proliferation of a cancer cell line is consistent with the observation that *NOV* expression level is increased in the senescing phase, which coincides with the low proliferative stage of hMSCs. Furthermore, in primary skin fibroblasts, *NOV/CCN3* protein increases the expression of human *SERPINE1* mRNA level (29). This is consistent with our observation that the expressions of *SERPINE1* as well as *NOV* are up-regulated during the late stages of cell culture. Mutant human *SERPINE1* (T333R; A355R), which lacks the protease-inhibitory activity, decreases the quantity of rat laminin and inhibits matrix accumulation (30). On the other hand, previous finding indicated that the expression of mouse *Myod1* (myogenic differentiation 1) mRNA level and Myog (myogenin) protein decreased in C2/4 cells (subclone of C2C12 mesenchymal cells) stably expressing *NOV*, which suggests that *NOV* suppresses the myogenic differentiation of C2/4 cells (31).

The expression of *RUNX2* was also decreased in late stage of the culture. *RUNX2* is a member of the runt family of transcription factors and suggested to be involved in osteogenesis (22). It is possible that down-regulated osteogenic differentiation of hMSCs is caused by the decreased expression of *RUNX2*. Recent reports have shown that 3D cultures of human adipose tissue-derived endothelial and osteoblastic progenitors generate osteogenic-vasculogenic constructs (32). It might be

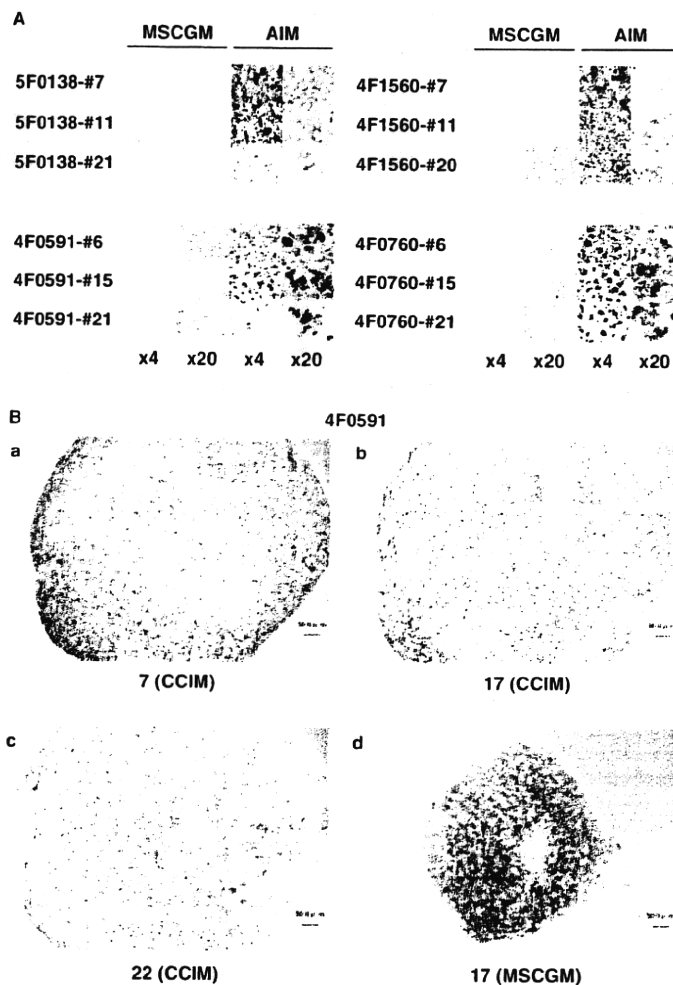


**Fig. 3. Adipogenic differentiation and chondrogenic differentiation of hMSCs.** (A) The cells in each passage numbers indicated were plated on 24-well plates and cultured in MSCGM (as control) or AIM (adipogenic differentiation medium) for 21 days. The cells were stained with Oil Red O.

(B) The cells in passage #7, #17 or #22 of 4F0591 were cultured in CCIM for 24 days and stained with Safranin O (a, b, c, respectively). Proteoglycans stained red. The cells in passage #17 were also cultured in MSCGM (as control) for 24 days (d).

interesting to investigate the gene expression profile of the 3D culture of hMSCs.

In conclusion, microarray and RT-PCR data of the six batches of hMSCs suggested that four genes, *EPHA5*, *NOV*, *NDN* and *RUNX2* have the potential to act as stage-specific markers during hMSC culture. These genes can be used as candidates for quality control markers of the culture status with regard to the differentiation potential for future clinical application of hMSCs for cellular therapeutics. We reported that the capacity of hMSCs for osteogenic differentiation was highly suppressed during the late culture stages. *NDN* or *RUNX2* may be a quality control marker of hMSC capacity for osteogenic differentiation. The observations of adipogenic differentiation of hMSCs suggested that each batch shows different transition in differentiation potential. It seemed that

the capacity tends to be suppressed in late stage of the culture. The observations of chondrogenic differentiation suggested that the differentiation potential of hMSCs is retained in late stage of the culture. It seems that the cells in the late stage have limited differentiation potential (oligopotent). Furthermore, network analysis and gene expression analysis revealed that the expression profiles are distinct for each passage number. These findings imply the importance of quality control for safe application of hMSCs for cellular therapy and usefulness of expression analysis for finding marker genes. Phenotype profiling and profiling at the genome level, including chromosomal analysis, might need more research in the future. The profiling of the cells, in both differentiated and 3D states, will also need to be investigated for future clinical applications.

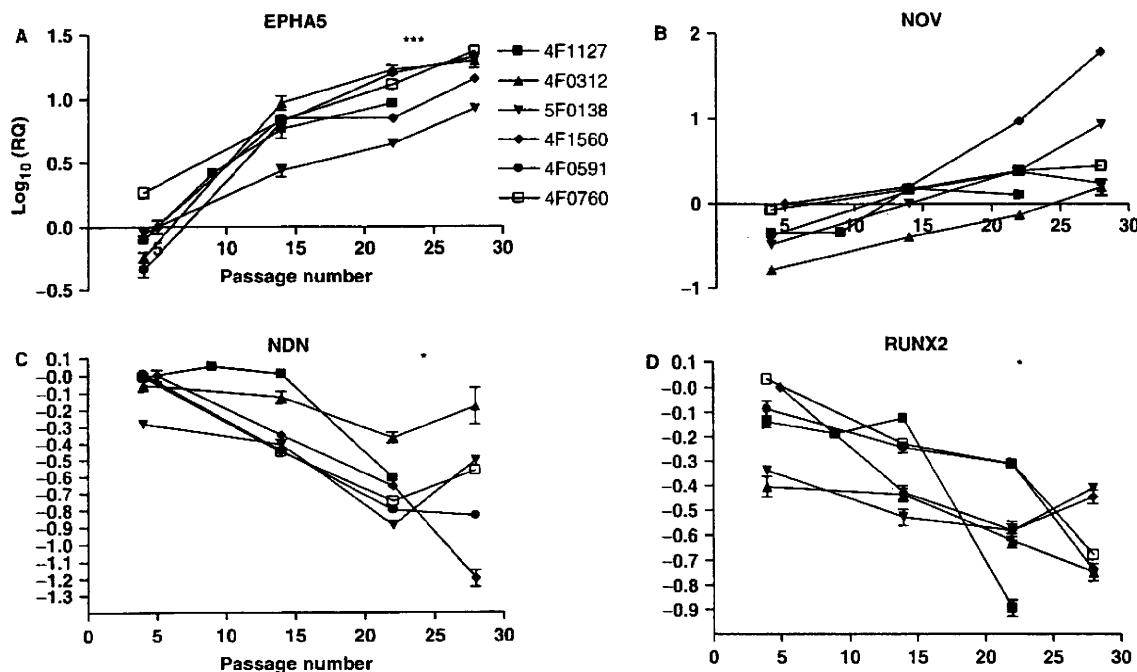


Fig. 4. Gene expression profiles of culture stage markers suggested for hMSCs. Individual plots for six batches of hMSCs obtained from RT-PCR data. The expression of *EPHA5* (A), and *NOV* (B) increased, while that of *NDN* (C) and *RUNX2* (D) decreased as the cells were further passaged in each batch.

Relative quantity value was plotted on a log 10 scale. The expression of four genes (A–D) was correlated with passage numbers ( $P < 0.01$ ). \*\*\*  $P < 0.001$ , \*  $P < 0.05$  when the expression in passage #14 was compared to that in late stage (passage #22 and #28) ( $n = 6$  in passage #14,  $n = 10$  in late stage).

Supplementary data are available at *JB* online.

We thank Dr Y. Hayashi for advice in microarray statistics analysis, and Dr Y. Shinozaki for assistance in microarray experiments. We are also thankful to Dr Y. Ohno and Dr E. Uchida for their support and valuable comments. We are most grateful to C. Aoyagi for her excellent skill in making paraffin sections. This work was supported in part by grants and the Grant-in-Aid for Cancer Research from the Ministry of Health, Labour and Welfare.

#### REFERENCES

- Clevers, H. (2005) Stem cells, asymmetric division and cancer. *Nat. Genet.* **37**, 1027–1028
- Takahashi, K., Tanabe, T., Ohnuki, M., Narita, M., Ichisaka, T., Tomoda, K., and Yamanaka, S. (2007) Induction of pluripotent stem cells from adult human fibroblasts by defined factors. *Cell* **131**, 861–872
- Fazel, S., Cimini, M., Chen, L., Li, S., Angoulvant, D., Fedak, P., Verma, S., Weisel, R.D., Keating, A., and Li, R.K. (2006) Cardioprotective c-kit<sup>+</sup> cells are from the bone marrow and regulate the myocardial balance of angiogenic cytokines. *J. Clin. Invest.* **116**, 1885–1877
- Rosenzweig, A. (2006) Cardiac cell therapy-mixed results from mixed cells. *N. Engl. J. Med.* **355**, 1274–1277
- Wollert, K.C., Meyer, G.P., Lotz, J., Lichtenberg, S.R., Lippolt, P., Breidenbach, C., Fichtner, S., Korte, T., Hornig, B., Messinger, D., Arseniev, L., Hertenstein, B., Ganser, A., and Drexler, H. (2004) Intracoronary autologous bone-marrow cell transfer after myocardial infarction: the BOOST randomised controlled clinical trial. *Lancet* **364**, 141–148
- Schächinger, V., Erbs, S., Elsässer, A., Haberbosch, W., Hambrecht, R., Holschermann, H., Yu, J., Corti, R., Mathey, D.G., Hamm, C.W., Suselbeck, T., Assmus, B., Tonn, T., Dimmeler, S., and Zeiher, A.M. (2006) Intracoronary bone marrow-derived progenitor cells in acute myocardial infarction. *N. Engl. J. Med.* **355**, 1210–1221
- Assmus, B., Honold, J., Schächinger, V., Britten, M.B., Fischer-Rasokat, U., Lehmann, R., Teupe, C., Pistorius, K., Martin, H., Abolmaali, N.D., Tonn, T., Dimmeler, S., and Zeiher, A.M. (2006) Transcatheter transplantation of progenitor cells after myocardial infarction. *N. Engl. J. Med.* **355**, 1222–1232
- Lunde, K., Solheim, S., Aakhus, S., Arnesen, H., Abdelnoor, M., Egeland, T., Endresen, K., Ilebakk, A., Mangschau, A., Fjeld, J.G., Smith, H.J., Taraldsrud, E., Grøgaard, H.K., Bjørnerheim, R., Brekke, M., Müller, C., Hopp, E., Ragnarsson, A., Brinchmann, J.E., and Forfang, K. (2006) Intracoronary injection of mononuclear bone marrow cells in acute myocardial infarction. *N. Engl. J. Med.* **355**, 1199–1209
- Janssens, S., Dubois, C., Bogaert, J., Theunissen, K., Deroose, C., Desmet, W., Kalantzi, M., Herbots, L., Sinnave, P., Dens, J., Maertens, J., Rademakers, F., Dymarkowska, S., Gheysens, O., Cleemput, J.V., Bormans, G., Nuyts, J., Belmans, A., Mortelmans, L., Boogaerts, M., and Van de Werf, F. (2006) Autologous bone marrow-derived stem-cell transfer in patients with ST-segment elevation myocardial infarction: double-blind, randomised controlled trial. *Lancet* **367**, 113–121